Plasmodium falciparum LipB mutants display altered redox and carbon metabolism in asexual stages and cannot complete sporogony in *Anopheles* mosquitoes

Marco Biddau[a,b,*], T.R. Santha Kumar[c], Philipp Henrich[c], Larissa M. Laine[b], Gavin J. Blackburn[d], Achuthanunni Chokkathukalam[d], Tao Li[e], Kim Lee Sim[e], Lewis King[a], Stephen L Hoffman[e], Michael P. Barrett[a,d], Graham H. Coombs[f], Geoffrey I. McFadden[g], David A. Fidock[c,h,1], Sylke Müller[b,1], Lilach Sheiner[a,b,*]

[a]*Wellcome Centre for Integrative Parasitology, University of Glasgow, Glasgow, United Kingdom*

[b]*Department of Infection, immunity and inflammation, University of Glasgow, Glasgow, United Kingdom*

[c]*Department of Microbiology and Immunology, Columbia University Irving Medical Center, New York, NY 10032, USA*

[d]*Glasgow Polyomics, Wolfson Wohl Cancer Research Centre, University of Glasgow, Glasgow, United Kingdom*

[e]*Sanaria Inc., Rockville, Maryland 20850, USA*

[f]*Strathclyde Institute of Pharmacy and Biomedical Sciences, University of Strathclyde, Glasgow, United Kingdom*

[g]*School of Botany, University of Melbourne, Parkville, VIC 3010, Australia*

[h]*Division of Infectious Diseases, Department of Medicine, Columbia University Irving Medical Center, New York, NY 10032, USA*

[1]These authors contributed equally.

*Corresponding authors.

E-mail addresses: Lilach Sheiner: lilach.sheiner@glasgow.ac.uk

Marco Biddau: mark.biddau@gmail.com

.

Abstract

Malaria is still one of the most important global infectious diseases. Emergence of drug resistance and a shortage of new efficient antimalarials continue to hamper a malaria eradication agenda. Malaria parasites are highly sensitive to changes in the redox environment. Understanding the mechanisms regulating parasite redox could contribute to the design of new drugs. Malaria parasites have a complex network of redox regulatory systems housed in their cytosol, in their mitochondrion and in their plastid (apicoplast). While the roles of enzymes of the thioredoxin and glutathione pathways in parasite survival have been explored, the antioxidant role of α-lipoic acid (LA) produced in the apicoplast has not been tested. To take a first step in teasing a putative role of LA in redox regulation, we analysed a mutant *Plasmodium falciparum* (3D7 strain) lacking the apicoplast lipoic acid protein ligase B (*lipB*) known to be depleted of LA. Our results showed a change in expression of redox regulators in the apicoplast and the cytosol. We further detected a change in parasite central carbon metabolism, with *lipB* deletion resulting in changes to glycolysis and tricarboxylic acid cycle activity. Further, in another *Plasmodium* cell line (NF54), deletion of *lipB* impacted development in the mosquito, preventing the detection of infectious sporozoite stages. While it is not clear at this point if the observed phenotypes are linked, these findings flag LA biosynthesis as an important subject for further study in the context of redox regulation in asexual stages, and point to LipB as a potential target for the development of new transmission drugs.

Keywords: *Plasmodium falciparum*, Malaria, Apicoplast, Metabolism, Antioxidant, Lipoic acid, Redox, Sporogony

1. Introduction

Malaria remains a tremendous threat to human health with 200 million infections resulting in 405,000 deaths in 2018 (World Health Organization, 2019), so it is imperative that we identify new antimalarial targets. One potential target is the parasite redox regulation system. *Plasmodium falciparum* is constitutively exposed in all stages of its complex life cycle to molecules that challenge its redox balance. Finding ways to disrupt this delicate balance hold promise for drug development. Indeed, in vitro experiments in which parasites were exposed to exogenous H_2O_2-generating systems proved lethal for intra-erythrocytic stages (Dockrell and Playfair, 1984). Similarly, mature gametocytes are sensitive to the oxidative stress generated by exposure to redox-cyclers in vitro (Siciliano et al., 2017). Finally, an animal diet that generates an environment rich in reactive oxygen species (ROS) in hepatocytes can reduce *Plasmodium* infection in vivo (Zuzarte-Luís et al., 2017). Despite this importance, and the fact that redox regulation is a fundamental aspect of cellular functions, our understanding of the parasite redox regulatory networks remains limited (Kehr et al., 2010; Müller, 2015).

The apicoplast, a non-photosynthetic plastid acquired via secondary endosymbiosis of a red algal cell, is an active metabolic hub in apicomplexan parasites including *Plasmodium* spp., (Sheiner et al., 2013; Mohring et al., 2014;Frohnecke et al., 2015; Kimata-Ariga et al., 2018; Biddau and Sheiner, 2019). In asexual red blood stages grown in culture, the apicoplast is essential only for the synthesis of isoprenoid precursors (Yeh and DeRisi., 2011). The apicoplast hosts components of the thioredoxin and the glutathione systems, which represent the two best characterized cellular antioxidant systems. Apicoplast-based redox regulators include the peroxiredoxin antioxidant protein (AOP), the dually-targeted (cytosol and apicoplast) enzymes glutathione reductase (GR), and the glutathione peroxidase-like thioredoxin peroxidase (TPx_{Gl}) (Kehr et al., 2010; Laine et al., 2015). Similarly, two glyoxalase system proteins are apicoplast targeted: glyoxalase-1-like protein (GILP), and glyoxalase 2 (tGloII) (Kehr et al., 2010; Urscher et al., 2010). Glyoxalase 2 is proposed to play a role in the

detoxification of incomplete triosephosphate-isomerase reaction products, but is apparently dispensable during intra-erythrocytic development (Wezena et al., 2017). Two additional apicoplast thioredoxin-like proteins (ATrx1 and ATrx2) are found in the peripheral compartments where they play an essential role in the control of protein sorting and folding in response to organelle redox status (Biddau et al., 2018). The *Plasmodium* orthologue of ATrx2 (*Pf*ATrx2; PF3D7_0529100) also appears to be essential (Bushell et al., 2017; Zhang et al., 2018). Many other potential redox-active proteins are predicted to be localised in the apicoplast (Boucher et al., 2018), but their roles are uncharacterized.

An additional molecule proposed to take part in apicoplast redox regulation is α-lipoic acid (LA) (Günther et al., 2007; Frohnecke et al., 2015; Laine et al., 2015). Due to its reducing properties, LA is known as the 'universal antioxidant' (Kagan et al., 1992; Perham, 2000; Gorąca et al., 2011; Moura et al., 2015; Tibullo et al., 2017). The proposed antioxidant role of LA in the apicoplast is based on a link between redox regulation and apicoplast pyruvate metabolism via the pyruvate dehydrogenase enzyme complex (PDC). The three enzymes in the PDC complex are pyruvate dehydrogenase (E1), dihydrolipoyl transacetylase (E2) and apicoplast dihydrolipoyl dehydrogenase (aE3). Through a series of reactions, PDC transfers an acetyl group from pyruvate to coenzyme A (CoA) to generate acetyl-CoA for the fatty acid biosynthesis pathway (Mooney et al., 2002; Foth et al., 2005) (Fig. 1). This activity depends on LA bound to the E2 lipoyl domain, which is reduced to dihydrolipoic acid (DHLA) during the process. The final reaction of *Plasmodium* PDC is catalysed by aE3, which re-oxidises DHLA back to LA to allow another cycle of PDC activity (Fig. 1). The activity of aE3 is coupled to the reduction of NAD^+ to $NADH+H^+$, which in turn takes part in apicoplast redox regulation (McMillan et al., 2005; Laine, L.M., 2014. Functional, biochemical and structural analyses of *Plasmodium falciparum* pyruvate dehydrogenase complex. PhD Thesis, University of Glasgow. University of Glasgow, UK). The DHLA/LA redox couple has a redox potential of -0.32 V, which is lower than the glutathione/glutathione disulphide (GSH/GSSG) couple

potential of -0.24 V, thus making glutathione a potential substrate for DHLA (Packer et al., 1995).

The apicoplast retains its exclusive LA biosynthesis pathway, catalysed by the enzymes octanoyl-ACP:protein *N*-octanoyltransferase (LipB) and lipoyl synthase (LipA) (Fig. 1), which operates independently from the mitochondrial LA salvage (Crawford et al., 2006; Günther et al., 2009). A *lipB* mutant was earlier generated and shown to have 90% LA depletion (Günther et al., 2007). As a first step to tackle the putative role of LA in redox regulation, we examined the changes in the expression of redox regulation enzymes in this *P. falciparum* mutant (named 3D7$^{\Delta PflipB}$). We also describe the metabolic changes occurring upon *lipB* deletion. As a comparison, we also analysed an aE3 deletion mutant that has only a mild effect on redox balance in the parasite (Laine et al., 2015), potentially because aE3 function might be compensated by alternative apicoplast enzymatic systems coupled to NAD(P)$^+$ reduction such as the NADP$^+$-specific glutamate dehydrogenase (Zocher et al., 2012). Our results describe a correlation between LA availability and redox regulation. Additionally, *lipB* deletion led to changes in central carbon metabolism. Finally, *lipB* deletion, generated in a separate NF54 line, hampers the ability of the parasites to develop in the mosquito, suggesting that LipB is essential in this life stage.

2. Materials and methods

2.1. Parasite culture and assessment of growth

2.1.1. Plasmodium falciparum culturing and synchronization

Plasmodium falciparum 3D7 parasites (isolated in the Netherlands) were cultured in RPMI 1640 (Invitrogen, UK) supplemented with 11 mM D-Glucose (Sigma Aldrich, UK), 0.5% w/v AlbuMAX II (Invitrogen, UK), 200 mM hypoxanthine (Sigma Aldrich, UK), and 20 mg/ml of gentamycin (PAA, Germany) in human erythrocytes at 5% haematocrit (Trager and Jensen,

1976). Parasites were cultured, maintaining a reduced oxygen atmosphere (1% O_2, 3% CO_2 and 96% N_2) and a constant temperature of 37°C (referred to as standard procedures). Parasitemias were determined by microscopy-based analysis of Giemsa-stained thin smears and synchronisations were performed following the sorbitol procedure (Lambros and Vanderberg, 1979). Tighter synchronisation was obtained by a combination of sorbitol treatment with magnetic-activated cell sorting (MACS) using LD columns (Miltenyi Biotech, Germany). Briefly, sorbitol-synchronised parasites were maintained in culture until they reached the early ring stage. Cultures were synchronised twice with sorbitol 6 h apart and then cultured until they reached the late schizont stage. Schizonts were purified over a MACS column once cultures had reached a schizont:ring ratio of 1:2. Schizonts were then placed in culture for 1 h with gentle shaking and cultures were synchronised again using the sorbitol method to obtain highly synchronous ring stages with 1 h synchrony. Highly synchronous parasites were used for all time point experiments and RNA extractions, with triplicate cultures for each condition.

2.1.2. Spent medium metabolite quantification

Analyses of D-glucose and L-lactate concentrations from spent culture medium samples were performed using the D-Glucose-HK and L-Lactic acid kits from Megazyme (Ireland) following the manufacturer's protocol. Briefly, parasite cultures for each condition were synchronised using a double sorbitol treatment (Lambros and Vanderberg, 1979) with a 6 h window, and split into triplicate cultures at the same parasitemia. At each time point, an aliquot of the culture was collected from each condition and erythrocytes were pelleted by centrifuging at 1000 *g* for 5 min. The resulting supernatant was then stored at -20°C. For the enzymatic assay, parasite spent medium samples were diluted by 1:6 with double distilled water.

155 *2.2. Evaluation of antioxidant gene expression*

156 *2.2.1. Reverse-Transcription quantitative PCR (RT-qPCR)*

157 Highly synchronous parasites (see section 2.1.1) were cultured in triplicate for each
158 condition until they reached 26, 30 and 34 h post-invasion (pi). Pellets of infected red blood
159 cells (RBCs) at 6-8% parasitemias were then washed three times in PBS and kept at -80°C.
160 Nucleic acids were extracted using the RNeasy kit (QIAGEN). Contaminating DNA was
161 removed using the Turbo DNA-free kit (Thermo Fisher Scientific). RNA samples were then
162 reverse transcribed using the RETRO-script kit (Thermo Fisher Scientific). Quantitative PCR
163 (qPCR) was performed using the Power SYBR Green Master Mix (Thermo Fisher Scientific,
164 UK) adding 20 ng of cDNA for each reaction and 300 nM of each primer (see Supplementary
165 Table S1). All reactions were run in a 7500 Real-Time PCR System (Applied Biosystems, UK).
166 The calculation of relative gene expression was performed using the ΔΔ(Ct) method (Livak
167 and Schmittgen, 2001).

168

169 *2.2.2. Protein extraction and quantitative fluorescent western blot*

170 For protein extraction, saponin-lysed parasite pellets were resuspended in 2D lysis
171 buffer (100 mM Hepes pH 7.4, 5 mM MgCl2,10 mM EDTA, 0.5% (v/v) Triton X-100, 5 µg/ml
172 of RNase A, 1x complete protease inhibitor cocktail (Roche, Switzerland) in double distilled
173 (dd)H_2O). Samples were subjected to three rounds of freezing and thawing on dry ice, and
174 incubated at 4°C for 5 min in a sonicated water bath. Samples were then centrifuged at 13,000
175 *g* for 20 min at 4°C. Supernatants containing protein fractions were quantified using the Protein
176 Assay kit (Bio-Rad, UK), with BSA used to generate a reference quantification curve.

177 Western blot analysis was performed by separating 20 µg of protein sample by SDS-
178 PAGE with NuPage Novex 4–12% and 15% (w/v) Bis-Tris gels (Invitrogen, UK). Separated
179 proteins were transferred to Protran nitrocellulose membranes (Schleicher & Schuell,

Germany) using a Transblot semi-dry transfer system (Bio-Rad, UK). Membranes were blocked with 5% (w/v) dried skimmed milk in PBS for 1-18 h and incubated for 1 h with two or more primary antibodies. Primary antibodies used for relative quantification included *P. falciparum* rabbit anti-actin antibody (1:12,000, loading control), *P. falciparum* rabbit anti-1-CysPx (1-Cys peroxiredoxin) antibody 1:50,000; *P. falciparum* rabbit anti-2-CysPx (2-Cys peroxiredoxin) antibody at 1:70,000; *P. falciparum* rabbit anti-BCKDH E2 antibody at 1:5,000; *P. falciparum* rabbit anti-isocitrate dehydrogenase antibody at 1:10,000 and *P. falciparum* rabbit anti-PDC E2 lipoyl domain antibody at 1:250. Membranes were washed three times in PBS containing 0.2% (v/v) Tween 20 and 2.5% (w/v) dried skimmed milk. Blots were then probed with infrared dye-conjugated antibody (1:10,000, IRDye800CW goat anti-rabbit antibody; LI-COR Biosciences, USA) for 1 h and washed again twice. Membranes were loaded in an Odyssey SA scanner (LI-COR Biosciences, USA) and fluorescent signal intensities quantified with the Image Studio software (LI-COR Biosciences, USA). All antibodies were custom made by Eurogentec.

2.3. Metabolomics experiment and analysis

2.3.1. ^{13}C-U-D-glucose labelling experiment setup

Parasites were cultured until parasitemias attained 6-8%. Two sorbitol treatments were performed at approximately 8 and 14 h pi. After synchronisation, triplicate parasite cultures were initiated using a medium where D-glucose was replaced with ^{13}C-U-D-glucose (99%, CK Gas Products Ltd, UK) and the haematocrit was set to 1%. A control culture of uninfected RBCs was prepared with the same conditions. All cultures were incubated for 20 h following standard procedures until late trophozoites. At this point, parasite culture metabolism was rapidly quenched at 4°C in a bath of dry ice and 70% ethanol (Vincent and Barrett, 2015). Erythrocyte pellets were then obtained and washed in ice-cold PBS by centrifugation at 800 *g* for 5 min at 4°C. Infected RBCs in the pellets were enriched using MACS LD column purification (Miltenyi Biotech, Germany) and a QuadroMACS magnet (Miltenyi Biotech,

Germany) with all steps performed at 4°C. Enriched samples were quantified using a Neubauer cell counting chamber and a Scepter 2.0 Handheld Automated Cell Counter (Millipore) to have 2.0×10^8 infected RBCs per sample. The same number of uninfected RBCs was collected as a control. All the samples were then added to a solution of HPLC-grade chloroform:methanol:water (1:3:1; v/v/v), at a concentration of $2x10^8$ parasites per 0.5 mL solution, incubated in ice in a sonicating water bath for 2 min and extracted for 1 h at 4°C and 1500 rpm on an orbital shaker. After extraction, samples were centrifuged at 13,000 *g* for 20 min at 4°C, and supernatants transferred into glass mass spectrometry vials (Thermo Fisher Scientific, UK) and stored at -80°C until LC-MS analysis.

2.3.2. LC-MS analyses

Metabolomics analyses were performed by LC-MS using an Ultimate 3000 LC system (Dionex, UK) connected to a Q Exactive HF Hybrid Quadrupole-Orbitrap mass spectrometer, (Thermo Fisher Scientific). The system was controlled by the software Chromeleon (Dionex, UK) and Xcalibur (Thermo Scientific), acquiring both positive and negative ionisation modes. Chromatographic separation was performed with a ZIC-pHILIC chromatography column (150mm (length) x 4.6mm (diameter) 5um (bead size) ; Sequant, Uemå, Sweden) using a two solvent system consisting of solvent A: 20 mM ammonium carbonate and solvent B: acetonitrile.

2.3.3. Metabolomic data analysis

Vendor-specific raw data were initially centroided and converted into the open format mzXML for subsequent processing. PeakML files (Scheltema et al., 2011) were then generated by extracting the chromatographic peaks contained in the mzXML files using the detection algorithm from XCMS (Tautenhahn et al., 2008). The data processing pipeline

mzMatch.R (Jankevics et al., 2012) was used to sort and combine all PeakML files corresponding to replicates and to exclude all non-reproducible data. Further steps of noise-filtering, gap-filling, and metabolite identification were performed on PeakML files utilising data obtained from metabolic standards run in parallel. For each metabolite of interest, the proportions of each isotopologue and its relative abundance in the sample were determined. The PeakML.Isotope.TargetedIsotopes function of mzMatch-ISO (Chokkathukalam et al., 2013) was used to scan the PeakML files for labelled metabolite quality and quantity. All metabolites of interest in this study were reliably identified by comparison of the chromatographic retention times and the m/z values with an authentic metabolic standard processed in parallel. These should be then considered as "identified compounds" or level 1 according to the Metabolomic Standard Initiative (Sumner et al., 2007). All metabolomics data was corrected for natural carbon isotope abundance and reagent impurity using the software IsoCor (Millard et al., 2019).

2.4. Double cross-over deletion of PfLipB in the NF54 strain by the Cre-loxP system

Plasmodium falciparum NF54 parasites were cultured in complete medium containing RPMI 1640 salts and 10% heat-inactivated human serum (Graves et al., 1984). The strategy for deleting *pflipB* using *Cre-lox*P is depicted in Supplementary Fig. S1. Briefly, we employed a double crossover recombination strategy to generate parasite lines lacking a functional *pflipB* locus (PlasmoDB ID: PF3D7_0823600). A 0.5 kb fragment of *pflipB,* PCR-amplified from NF54 genomic DNA using primers p1/p2 (Supplementary Table S1), was cloned into PCC1-*cdup*-h*dhfr*-DXO between the *Sac*II and *Afl*II sites and served as the homology region for the first cross-over (O'Neill et al., 2011). The second homologous fragment (0.5 kb) was PCR-amplified using primers p3/p4 and cloned between *Eco*RI and *Avr*II sites to give rise to an 8.5 kb PCC1-*cdup*-h*dhfr*-Δ*lipB* plasmid. Fifty μg of this plasmid was used to transfect NF54 parasites by electroporation and transformed parasites were selected with 1.5 nM WR99210.

Drug pressure was maintained for 7 days and parasites were then cultured in drug-free medium up to day 27 when WR99210-resistant parasites appeared. Resistant parasites were then treated with 1.0 μM 5-Fluorocytosine (in DMSO) to remove single crossover-integrated plasmid and episomal forms, both of which contain the *cdup* negative selection marker (Maier et al., 2006). PTET-BSD-*Cre* (a kind gift from Alan Cowman, Walter and Eliza Hall Institute, Australia) was transfected into recombinant NF54 parasites and cultured in 2.5 μM blasticidin S-hydrochloride for 7 days, after which single-cell cloning was performed (Goodyer and Taraschi, 1997).

2.5. Generation of Pf∆lipB gametocytes and production of salivary gland sporozoites

Gametocytes were induced from *Pf∆lipB* and wild-type (WT) NF54 parasite lines by multiple rounds of sub-culturing for 14-18 days with nutrient deprivation, as described (Ponnudurai et al., 1986). Gametocyte induction and maturation was monitored microscopically by Giemsa-stained thin blood smears from culture samples. Mature gametocyte pellets were mixed with fresh O-type Rh^+ blood and human serum to produce an artificial blood meal at approximately 50% hematocrit for mosquito feeds. The final concentration of stage V gametocytes in artificial blood meals was 1.0%±0.1% (mean ± S.E.M. across seven experiments), which was equivalent to the gametocyte numbers observed with NF54 parasites (Supplementary Table S1). *Anopheles stephensi* mosquitoes were fed 3-5 days after their emergence from pupae. Fed mosquitoes were maintained for 13–16 days before recovery of salivary gland sporozoites (SPZ) by hand dissection.

2.6. Ultrastructural analysis of midgut oocysts

The infected midgut oocysts were fixed in 4%/0.1% formaldehyde/glutaraldehyde and immersed in a 50:50 glycerol/water solution for Differential Interference Contrast (DIC)

imaging. Using a Nikon Ti Eclipse inverted microscope, cut midgut sections were pre-screened for the presence of oocysts at 10× magnification using an automated tiling feature of the Nikon NIS Elements 3.2 software. Individual oocysts were imaged at high magnification using a 60× NA 1.4 oil immersion objective with a matching DIC slider. Images were compiled using the National Institute of Health (USA) ImageJ program (https://imagej.nih.gov/ij).

Morphology of developing oocysts was examined by fixing dissected mosquito midguts in 2.5% glutaraldehyde in PBS, and then in 0.5% OsO_4, dehydration in an ethanol series, embedding in London Resin White, and semi-thin sections (400 nm) were mounted on glass slides and stained with 0.5% toluidine blue (w/v): 0.1% Na_2CO_3 (w/v) for 10 s, and then imaged on an Olympus BH-2 light microscope.

3. Results

3.1. Deletion of lipB results in accelerated differentiation and changes in apicoplast and cytosol antioxidant levels

Pronounced LA deficiency was previously detected in the trophozoite stage in *lipB* knockout (KO) line $3D7^{\Delta PflipB}$ parasites (Günther et al., 2007). The LA depletion seen in this mutant provided an opportunity to take the first steps to investigate whether this deficiency affected the apicoplast antioxidant composition. We monitored the relative transcription levels of genes encoding apicoplast antioxidants at 26, 30 and 34 h pi by qPCR for both $3D7^{\Delta PflipB}$ and the parental ($3D7^{WT}$) parasites. We used primer sets to specifically quantify the transcripts of the apicoplast redox-active proteins TPx_{Gl} (PF3D7_1212000), ATrx2 (PF3D7_0529100) and AOP (PF3D7_0729200) (Fig. 2A), which take part in the thioredoxin redox system, and the apicoplast glyoxalase system proteins GILP (PF3D7_0604700) and tGlo (PF3D7_1205700) (Supplementary Fig. S2). Among these, TPx_{Gl} had the largest change in expression levels, with relative transcription levels displaying three to four-fold increases at 30

h pi and 34 h pi compared with 3D7^{WT}. Similarly, ATrx2 relative expression showed a four-fold increase compared with the 3D7^{WT} parasites at 26 h pi followed by a two-fold decrease at 34 h pi, when AOP also showed a two-fold decrease (Fig. 2A). In contrast, the apicoplast glyoxalase system enzymes presented no significant differences in relative expression (Supplementary Fig. S2).

In light of these observed changes in apicoplast antioxidant expression, we wanted to test whether the cytosolic antioxidant composition was also affected. Therefore, we used quantitative fluorescent western blotting to monitor the relative levels of GST (PF3D7_1419300), 1CysPx (PF3D7_0802200) and 2-CysPx (PF3D7_1438900). These proteins were measured in 3D7$^{\Delta PflipB}$ and 3D7^{WT} late trophozoites at 34 h pi. We observed a significant two-fold increase in protein levels for GST and 1-CysPx in 3D7$^{\Delta PflipB}$ mutants (Fig. 2B, Supplementary Fig. S3). Conversely, 2-CysPx levels appeared to remain unchanged between the two lines (Fig. 2B).

In a previous study, *lipB* deletion was reported to result in a slight increase in parasite growth in culture (Günther et al., 2007). We examined the effect on asexual cycle progression in more detail and found that at 30 h pi the 3D7$^{\Delta PflipB}$ mutant showed an increase in differentiation into schizonts with a 6 h advance compared with 3D7^{WT} (Fig. 2C). This accelerated differentiation resulted in faster completion of the trophozoite stage and of the whole asexual cycle but had no effect on the average number of merozoites (Fig. 2D).

These finding provide indirect evidence of a change in the underlying redox potential of both the apicoplast and the cytosol upon *lipB* deletion at the time points examined. It remains to be determined whether the redox changes observed occur as a result of the shorter differentiation window or are the cause for it. The detection of some changes in redox regulators starting at 26 h pi, 4 h prior to the observed accelerated differentiation, suggests the latter.

3.2. Deletion of lipB affects parasite carbon metabolism

In eukaryotic cells, the compartmental redox state and the availability of redox conducting and regulating molecules in different cellular compartments are intertwined with the activity of metabolic pathways. The redox conditions in a cellular compartment affect the function of its metabolic enzymes, while in turn, the metabolic reactions in a compartment generate metabolites that impact its redox state. Thus, we proceeded to examine whether the observed redox changes in 3D7$^{\Delta PflipB}$ mutants coincide with changes in central carbon metabolism. We chose to make this analysis alongside a *P. falciparum* apicoplast dihydrolipoamide dehydrogenase (aE3) knock-out mutant (3D7$^{\Delta Pfae3}$) (Laine et al., 2015). Unlike 3D7$^{\Delta PflipB}$, the deletion of a PDC component in 3D7$^{\Delta Pfae3}$ does not result in disruption of LA biosynthesis nor of PDC activity, and its effect on the expression of redox regulators is only mild (Laine et al., 2015), which makes 3D7$^{\Delta Pfae3}$ a relevant negative control.

The levels of D-glucose and L-lactate in spent medium were monitored using commercial enzymatic assays in two independent experiments. As glycolytic activity in *P. falciparum* typically peaks during intra-erythrocytic trophozoite development (Shivapurkar et al., 2018), we collected samples at 30, 34, 38 and 42 h pi to cover this developmental stage. Results showed that spent medium samples from 3D7$^{\Delta PflipB}$ contained significantly less D-glucose (Fig. 3A) and more L-lactate (Fig. 3B) than 3D7^{WT} at 42 h pi. Conversely, 3D7$^{\Delta Pfae3}$ mutants did not present this trend and the concentrations for these metabolites in spent medium were comparable to the WT controls (Supplementary Fig. S4).

We further hypothesised that the up-regulation of glycolysis and the change to antioxidant expression described above might affect downstream metabolism and especially the tricarboxylic acid (TCA) cycle. Therefore, we proceeded to set up two steady-state targeted metabolomics experiments in technical triplicates, using the isotope-labelled nutrient ^{13}C-U-D-glucose. 3D7$^{\Delta PflipB}$ and 3D7^{WT} parasites were synchronised and metabolically labelled for 28 h. Parasites at the late trophozoite stage were then rapidly chilled, and the extracted

359 metabolites analysed by LC-MS to follow [^{13}C] labelling. In agreement with the observation
360 from the spent medium, 3D7$^{\Delta PflipB}$ mutants displayed a two-fold increase in the relative levels
361 of the glycolytic metabolite pyruvate and of glycerol-3-phosphate, which derive from a
362 glycolytic intermediate (Fig. 4A, Ba). A similar trend was also displayed by the metabolites 2-
363 oxoglutarate and succinate associated with the TCA cycle, as well as the amino acid
364 aspartate, whereas alanine showed a reduction in relative intracellular level (Fig. 4A, B). The
365 analysis of the labelled fraction for these metabolites showed an immediate conversion of
366 glucose into glycolytic intermediates (Supplementary Fig. S5), in line with previous analyses
367 (Storm et al., 2014). Conversely, the analysis of 3D7$^{\Delta Pfae3}$ mutants showed no significant
368 differences in the relative abundances for these metabolites (Fig. 4C).

369 Only a small fraction of [^{13}C] labelled triose phosphates was fed into the TCA cycle
370 intermediates in all three parasite lines (Supplementary Fig. S5), as has been well established
371 in the literature (MacRae et al., 2013; Storm et al., 2014; Ke et al., 2015). Interestingly,
372 whereas the 3D7^{WT} control had M+4, M+5 and M+6 citrate labelling, indicative of a complete
373 TCA cycle activity, this was not the case for 3D7$^{\Delta PflipB}$. Rather, in 3D7$^{\Delta PflipB}$ signals for M+4 and
374 M+6 citrate were below the detection level, while the M+5 fraction was significantly decreased
375 (Fig. 4D). In both the experiments an increment of M+2 citrate was detected for 3D7$^{\Delta PflipB}$
376 mutants compared with 3D7^{WT}, however, with high variability between the two experiments
377 (Fig. 4D). These changes were not observed for 3D7$^{\Delta Pfae3}$ mutants (Fig. 4E). In the 3D7$^{\Delta PflipB}$
378 mutant, the presence of M+2 label in citrate suggests an unchanged flux of glycolytic pyruvate
379 into the TCA cycle. Conversely, the absence of M+4 and M+6 citrate isotopologues might lead
380 to a non-cyclic activity of the cycle, unlike that seen in 3D7^{WT} and 3D7$^{\Delta Pfae3}$. These
381 observations are similar to the phenotype found upon deletion of aconitase reported within a
382 study that provided a detailed analysis of the *P. falciparum* TCA cycle (Ke et al., 2015). The
383 significant reduction in the M+5 citrate fraction could be interpreted as a reduction in carbon
384 fixation activity by the PEP carboxylase branch. This observation is also supported by a
385 decrease in M+3 labelling for the metabolites malate and fumarate (Fig. 4D). Conversely, no

variations in malate and fumarate labelling were observed in the 3D7$^{\Delta PfAE3}$ mutants. To further investigate these variations in the TCA cycle activity in 3D7$^{\Delta PflipB}$, we performed quantitative western blot analysis of the enzymes operating the first steps of the TCA cycle. Interestingly, the 3D7$^{\Delta PflipB}$ mutant up-regulated the branched-chain α-keto acid dehydrogenase (BCKDH) component E2, the first enzyme converting pyruvate to acetyl-CoA (Oppenheim et al., 2014), while its apicoplast parallel PDC E2 displayed no significant difference in abundance (Fig. 5A, Supplementary Fig. S6). Additionally, isocitrate dehydrogenase (ICDH), which operates three steps downstream in the TCA cycle, displayed no differences in abundance compared with 3D7^{WT} (Fig. 5A, Supplementary Fig. S6). These variations in enzyme expression require further analysis. In light of the described increased glycolytic activity, an up-regulation of BCKDH might be required to sustain the flux of acetyl-CoA in the TCA cycle. The unaltered levels of ICDH contrast with the possible reduced conversion of isocitrate to 2-oxoglutarate in 3D7$^{\Delta PflipB}$, suggested by the observed variations in citrate labelling (Fig. 4D).

Lastly, we tested cofactors involved in carbon and energy metabolism, where we observed a decrease in relative intracellular levels of ATP in 3D7$^{\Delta PflipB}$ parasites, while all other cofactors tested were unchanged (Fig. 5B). In addition, 3D7$^{\Delta PflipB}$ mutants had an increase in the ADP M+5 fraction (Fig. 5C). These results might suggest an increased ATP demand in the mutants, possibly linked to the accelerated differentiation (Fig. 2C), although this explanation remains to be demonstrated directly. In summary, the analysis of 3D7$^{\Delta PflipB}$ mutant metabolism reveals an effect on the activity of both glycolysis and the TCA cycle. The specificity of this phenotype compared with 3D7$^{\Delta PfAE3}$ metabolism (Fig. 4Bb, Cb) provide indirect support to the possibility that there is a link between LA depletion and the observed changes.

3.3. A LipB mutant cannot complete development in a mosquito

411 We further investigated the development *of lipB*-deleted parasites in mosquitoes. For
412 this analysis, a second *lipB* deletion line was generated by double-crossover gene deletion
413 (Supplementary Fig. S1) in the NF54 background (NF54$^{\Delta PflipB}$), which is superior to 3D7
414 parasites in its ability to infect mosquitoes. Parasites were maintained in media containing
415 10% human serum, with the aim of them retaining their capacity to form mature gametocytes.
416 The deletion of *lipB* did not appear to overtly influence sexual commitment in the parasites
417 and mature gametocytes developed as in NF54^{WT} (Table 2, Fig. 6). This allowed us to proceed
418 to evaluate parasite development in the mosquito. Seven mosquito infection experiments were
419 performed with NF54$^{\Delta PflipB}$ gametocytes (Table 2). While midgut oocysts were detectable in all
420 experiments (Table 2), no sporozoites were detected in any of the infected mosquitoes in any
421 of the seven experiments, while an average of 136,922 ± 17,717 sporozoites were detected
422 in four mosquito infection experiments performed with the parental NF54 (Table 2, Fig. 6).
423 These data indicated a major defect in development in the mosquito in the NF54$^{\Delta PflipB}$
424 parasites. To explore this further, we examined the morphology of the midgut oocysts, and
425 found that the NF54$^{\Delta PflipB}$ oocysts present an unusual morphology (Fig. 7), which may be
426 suggestive of an attenuated sexual development for this line that could not complete its
427 transmission cycle in the *Anopheles* vector.

428

429 **4. Discussion**

430 The cellular redox balance of *Plasmodium* parasites is constantly under threat of
431 oxidative stress generated by the metabolic functions of the parasite and by the metabolic
432 activities and defence mechanisms of the host (Becker et al., 2004; Nepveu and Turrini, 2013;
433 Patzewitz et al., 2013; Müller, 2015). Apicoplast-specific redox balance is an integral part of
434 the overall cellular redox steady-state (Kehr et al., 2010; Mohring et al., 2017; Biddau et al.,
435 2018). While fragmented information is available about the different apicoplast redox control
436 pathways, their importance is evident in the series of specific antioxidant systems it hosts

(Kehr et al., 2010) and in the redox regulators controlling its biogenesis (Biddau et al., 2018). Similarly, apicoplast-hosted pathways are coupled to redox reactions, including the biosynthesis of isoprenoid precursors, which is coupled to the reduction of $NADP^+$ to NADPH plus H^+ (Seeber et al., 2005; Seeber and Soldati-Favre, 2010), and the activity of PDC as discussed here (Fig. 1). LA is proposed to contribute to redox regulation in other systems (Tibullo et al., 2017). The results presented here describing the phenotypes of *lipB* deletion provides preliminary evidence in support of this role within the apicoplast of *Plasmodium*, albeit indirect.

LA is a powerful antioxidant with low redox potential (Packer et al., 1995; Bilska and Włodek, 2005), which prompted us to test how interfering with LA biosynthesis affected apicoplast redox regulation. As a means to address this question, and in the absence of a method to directly and specifically deplete LA from the apicoplast, we examined the phenotypes of a *lipB* deletion mutant (3D7$^{\Delta PflipB}$) where 90% reduction of LA was earlier reported (Günther et al., 2007). We detected transcriptional changes of the apicoplast redox enzymes peroxidase-like enzyme TPx_{Gl}, thioredoxin ATrx2, and the peroxiredoxin AOP (Fig. 2A). We cannot exclude that these observations are a result of other outcomes of *lipB* deletion not related to LA depletion. Nevertheless, we propose the hypothesis that the observed redox changes might promote apicoplast redox homeostasis in response to an oxidative stress that may be caused by the depletion of the LA antioxidant function. In support of this hypothesis, up-regulation of TPx_{Gl} also occurs in response to other oxidative stresses in *P. falciparum* (Akide-Ndunge et al., 2009). Similarly, we recently reported that the ortholog of *Pf*ATrx2 in the related parasite *Toxoplasma gondii* (*Tg*ATrx2) controls apicoplast gene expression, likely via a redox state-controlled interaction with proteins in transit to the apicoplast lumen (Biddau et al., 2018). If *Pf*ATrx2 performs a similar function, then the changes in its expression in 3D7$^{\Delta PflipB}$ may serve to control protein transit to the apicoplast lumen in response to organelle redox imbalance. The different roles of TPx_{Gl} and ATrx2 may account for the different pattern in their transcriptional changes. This proposed putative role for LipB and, potentially, for LA

synthesis, in the maintenance of apicoplast redox balance raises the possibility, while speculative, that the apicoplast *Pf*PDC E2 enzyme may operate as an apicoplast antioxidant through its prosthetic LA. Examples of DHLA acting as an electron donor to both GSH and thioredoxin systems have been previously described in other organisms (Packer et al., 1995). DHLA bound to PDC-E2 and to α-ketoglutarate dehydrogenase (KGDH) acts as an electron donor to glutaredoxins in an *Escherichia coli* mutant where both the thioredoxin and the GSH systems were disrupted (Feeney et al., 2011). Similarly, *Mycobacterium tuberculosis* KGDH E2 uses DHLA to transfer electrons received from E3 to peroxiredoxins and contributes to antioxidant defence (Bryk et al., 2002). Additionally, KADH E2-mediated reduction of thioredoxins was observed in mammals (Bunik and Follmann, 1993). A similar redox regulatory role of the apicoplast PDC E2 may explain why it is expressed during the intra-erythrocytic stages (Foth et al., 2005; McMillan et al., 2005), despite the dispensability of fatty acid biosynthesis in this stage (Vaughan et al., 2009). Our attempts to delete PDC E2 in *P. falciparum* using gene replacement were unsuccessful (data not shown), raising the possibility that its role during intra-erythrocytic development is essential. In agreement with this observation, *Pfpdce2* was proposed to be essential during intra-erythrocytic development in a recent whole-genome random mutagenesis screen for *P. falciparum* (Zhang et al., 2018), however, *Pbpdce2,* was not found to be essential in a genome-wide screen performed for *Plasmodium berghei* (Bushell et al., 2017). This hypothetical role for *lipB,* and potentially LA, in redox regulation raises questions about the sources of electrons for LA/DHLA recycling. This might not be attributed exclusively to the flux of glycolytic pyruvate to PDC as this was suggested to contribute to a build-up of acetyl-CoA in the organelle (Lim and McFadden, 2010). A possible alternative candidate for LA/DHLA recycling might be the apicoplast-targeted GSH reductase (GR) (Müller, 2015). The GR-mediated reduction of LA was demonstrated in rats and, in particular, the use of NADPH $+H^+$ as an electron donor was described in mitochondrial fractions (Pick et al., 1995; Haramaki et al., 1997).

Our data identified changes in cytosolic antioxidant expression in 3D7$^{\Delta PflipB}$ parasites. Both enzymes for which we observed upregulation, GST and 1-CysPx (Fig. 2B), are highly abundant in the *P. falciparum* cytosol (Liebau et al., 2002), and both have demonstrated antioxidant activity in this compartment (Krnajski et al., 2001; Harwaldt et al., 2002; Liebau et al., 2002; Deponte and Becker, 2005). One potential explanation for this phenotype might be that a plastid-to-cytosol redox signalling, such as the signalling described in plant chloroplasts and cytosols (reviewed in Dietz et al., 2016) might also exist in *Plasmodium.* Testing this possibility will require further experimentation. In *Arabidopsis thaliana,* chloroplast-originated H_2O_2 signal induces upregulation of the expression of genes encoding different GSTs as well as enzymes involved in glycolysis and the pentose phosphate pathway (PPP) (Sewelam et al., 2014). Moreover, chloroplast-originated ROS signalling induces changes in the cell cycle progression (Bode et al., 2016).

The hypothesis that plastid-to-cytosol redox signalling occurs in *Plasmodium* is an exciting one which we think the field should consider in future work. Nevertheless, it is important to notice that while generating *lipB* deletion mutants, the parasites were forced through an intense selection bottleneck, and it is not possible to exclude that the observed redox changes may have resulted from adaptation that could have occurred during this process. In the future, it would be interesting to explore this hypothesis further using conditional mutants that would circumvent this complication and that may allow a temporal control of LA depletion.

Because we wanted to examine metabolic changes that might be linked to redox changes, we compared the metabolites between two mutants of the apicoplast PDH complex that show strong (*lipB* our study) or mild (aE3, (Laine et al., 2015)) changes in the expression of redox regulators. Metabolic analysis of 3D7$^{\Delta PflipB}$ mutants highlighted increased glycolytic activity, which is the main energy releasing pathway in blood stage *P. falciparum* (Salcedo-Sora et al., 2014). Increased glycolytic activity in the 3D7$^{\Delta PflipB}$ mutant was mostly evident

516 through increased glucose demand and increased lactate production via spent medium
517 analysis (Fig. 3) and was not seen in 3D7$^{\Delta Pfae3}$ parasite (Supplementary Fig. S4).

518 As it stands, these observations and the changes in redox regulators are linked to the
519 deletion of *lipB*. However, we propose one possible model that could be considered for tying
520 together the phenotypes of *lipB* deletion in the asexual stages: *lipB* deletion leads to LA
521 depletion; changes to apicoplast redox balance due to this depletion of LA might induce
522 changes in cytosolic redox through plastid-to-cytosol signalling as seen with other plastids.
523 This putative signal leads to the temporary accelerated differentiation observed (Fig. 2C),
524 which may be linked to the observed metabolic changes during the time window examined.
525 Some uncertainty with this model stems from the potential dual roles of LA in (i) potentially
526 regulating redox and (ii) supporting PDC-dependent fatty acid synthesis. However,
527 accumulating evidence suggests that the latter is not essential during intra-erythrocytic
528 development (Yeh and DeRisi., 2011; Cobbold et al., 2013) unless fatty acid starvation occurs
529 (Botté et al., 2013). We thus propose that the changes in carbon metabolism observed upon
530 *lipB* deletion are not the consequence of disruption of fatty acid metabolism. That said, we
531 cannot rule out that the changes in cytosolic redox regulator expression, asexual cycle
532 progression and the metabolic changes taking place in this mutant are not the cause of other
533 outcomes of the *lipB* deletion not yet identified.

534 *Plasmodium falciparum* asexual blood stages are characterised by an oxidative TCA
535 cycle, where the main carbon source is provided by 2-oxoglutarate that originates from
536 glutamine. The majority of these glutamine-derived carbons exit the cycle as malate, while
537 only a small fraction is further oxidised to generate oxaloacetate and citrate that then can take
538 part again in the cycle (Cobbold et al., 2013; MacRae et al., 2013; Ke et al., 2015). Comparing
539 the TCA cycle metabolism of 3D7$^{\Delta PflipB}$ mutants with 3D7^{WT} parasites revealed differences in
540 the glucose-derived carbon input. In 3D7$^{\Delta PflipB}$ mutants, citrate presented mainly as M+2
541 labelling and showed a significant decrease in M+5 while all other isotopologues for this
542 metabolite were below detection levels (Fig. 4D). These results suggest that citrate is likely

543 mainly generated by unlabelled oxaloacetate that originated from anaplerotic unlabelled 2-
544 oxoglutarate entering the TCA cycle and fully labelled pyruvate providing M+2 acetyl-CoA (Fig
545 4A). This observation and the apparent absence of M+4 and M+6 citrate isotopologues could
546 suggest that that the small fraction of glucose-derived carbon is not taking part in the full cycle
547 of 3D7$^{\Delta PflipB}$ mutants, unlike what happens in 3D7^{WT} parasites (Fig. 4D).

548 The link between *lipB* deletion and the changes seen in the TCA cycle requires further
549 study, and the lack of change in ICDH protein levels (Fig. 5A, Supplementary Fig. S6) is
550 puzzling. One possible explanation is that the enzymatic activity of ICDH, or indeed citrate
551 synthase and aconitase, may be inhibited in response to the observed cellular redox changes.
552 Studies on plant mitochondria highlight the role of thiol redox switches in adjusting
553 mitochondrial function in light of external stresses (reviewed in Nietzel et al., 2017), and citrate
554 synthase, aconitase and ICDH are all substrate for thiol based redox regulation (Yoshida et
555 al., 2013; Schmidtmann et al., 2014; Yoshida and Hisabori, 2014).

556 Interestingly, alongside the altered levels of citrate labelling, we observed an increase
557 in relative levels of BCKDH E2 (Fig. 5A) and no change in the total relative intracellular levels
558 of citrate (Fig. 4B). Previous studies suggested that citrate could take part in a malate shuttle,
559 whereby cytosolic citrate is used to generate oxaloacetate and acetyl-CoA, which in turn take
560 part in carbon fixation and protein acetylation (Cobbold et al., 2013; Storm et al., 2014). The
561 apparent absence of M+4 and M+6 citrate in 3D7$^{\Delta PflipB}$ mutants is in line with this scenario and
562 could suggest that the citrate fraction that is not cycling in the TCA cycle but may instead be
563 channelled towards this citrate shuttle. If true, this would result in increased availability of
564 cytosolic acetyl-CoA, which in turn may affect histone acetylation and thus gene expression
565 patterns (Cobbold et al., 2016). Similarly, in macrophages activated by LPS and IFNγ,
566 variations in the TCA cycle activity was observed along with reduced ICDH enzyme with
567 consequent accumulation of citrate and succinate, generation of ROS signalling, and
568 modulation of gene expression by alternative acetylation (Seim et al., 2019), lending
569 precedence to our proposed explanation. This scenario remains, nonetheless, a speculative

model that, if true, would explain the altered progression through the *P. falciparum* cell cycle, which typically depends on very tight regulation of gene expression (Bozdech et al., 2003).

We were unable to detect sporozoites in the salivary glands of mosquitoes infected with the NF54$^{\Delta Pflipb}$ mutant, despite the fact that normal numbers of oocysts were produced (Table 2, Fig. 6). This observation suggests that *lipB* is essential for successful sporogony. This finding is surprising considering the evidence from the rodent parasite *P. berghei*, where deletion of *lipB* caused no defect to the production of salivary gland sporozoites but showed a moderate defect in liver-stage development (Falkard et al., 2013). This is not the first example of such a discrepancy. PDC E1α is dispensable for mosquito development in the rodent malaria parasite *P. yoelii* but was necessary for sporozoite maturation in *P. falciparum* (Cobbold et al., 2013). These findings point to different dependencies of human and rodent malaria on PDC enzymes for development in the mosquito. A possible reason for this difference may be the increased number of sporozoites produced per oocyst, which is four-fold higher in the human malaria parasite *P. falciparum* (Rungsiwongse and Rosenberg, 1991) than in rodent malaria parasites (Lindner et al., 2013; Shimizu et al., 2010). High sporozoite numbers in rodent malaria oocysts may require enhanced metabolism, which would depend on both PDC activity and a functional redox regulation network. Future examination of the asexual stages of the NF54$^{\Delta Pflipb}$ mutant, such as the work presented here for the 3D7$^{\Delta PflipB}$ mutant, is merited to address the possibility that LA synthesis in the apicoplast is essential for completion of *P. falciparum* development in the mosquito vector.

Acknowledgements

We would like to thank Dr Sujaan Das, Dr Mahmood Alam and Dr Sonal Sethia for their help and advice. The research was supported by the European Community's Seventh Framework Programme [grant number FP7/2007-2013] under grant agreements No 242095 and No ParaMet 290080 (MB), by Medical Research Council, UK, grant number

596 MR/S024573/1 (LS), and by the National Institute of Health (USA) (R01 AI085584 to DAF).
597 The Wellcome Centre for Integrative Parasitology, UK, is supported by core funding from the
598 Wellcome Trust, UK [104111]. DAF gratefully acknowledges earlier funding from the NIH (R01
599 AI085584). Finally, GIM was awarded a Laureate Fellowship from the Australian Research
600 Council and LS is a Royal Society of Edinburgh Personal Research Fellow, UK.

601

602 **References**

603 Akide-Ndunge, O.B., Tambini, E., Giribaldi, G., McMillan, P.J., Müller, S., Arese, P.,
604 Turrini, F., 2009. Co-ordinated stage-dependent enhancement of *Plasmodium*
605 *falciparum* antioxidant enzymes and heat shock protein expression in parasites
606 growing in oxidatively stressed or G6PD-deficient red blood cells. Malar. J. 8, 113.
607 doi:10.1186/1475-2875-8-113

608 Becker, K., Tilley, L., Vennerstrom, J.L., Roberts, D., Rogerson, S., Ginsburg, H.,
609 2004. Oxidative stress in malaria parasite-infected erythrocytes: Host-parasite
610 interactions. Int. J. Parasitol. doi:10.1016/j.ijpara.2003.09.011

611 Biddau, M., Bouchut, A., Major, J., Saveria, T., Tottey, J., Oka, O., Van-Lith, M.,
612 Jennings, K.E., Ovciarikova, J., DeRocher, A., Striepen, B., Waller, R.F., Parsons,
613 M., Sheiner, L., 2018. Two essential Thioredoxins mediate apicoplast biogenesis,
614 protein import, and gene expression in *Toxoplasma gondii*. PLoS Pathog. 14,
615 e1006836. doi:10.1371/journal.ppat.1006836

616 Biddau, M., Sheiner, L., 2019. Targeting the apicoplast in malaria. Biochem. Soc.
617 Trans. 47, 973–983. doi:10.1042/BST20170563

618 Bilska, A., Włodek, L., 2005. Lipoic acid - the drug of the future? Pharmacol. Rep. 57,
619 570–7.

620 Bode, R., Ivanov, A.G., Hüner, N.P.A., 2016. Global transcriptome analyses provide
621 evidence that chloroplast redox state contributes to intracellular as well as long-
622 distance signalling in response to stress and acclimation in *Arabidopsis*.
623 Photosynth. Res. 128, 287–312. doi:10.1007/s11120-016-0245-y

624 Botté, C.Y., Yamaryo-Botté, Y., Rupasinghe, T.W.T., Mullin, K.A., MacRae, J.I.,

625 Spurck, T.P., Kalanon, M., Shears, M.J., Coppel, R.L., Crellin, P.K., Maréchal, E.,
626 McConville, M.J., McFadden, G.I., 2013. Atypical lipid composition in the purified
627 relict plastid (apicoplast) of malaria parasites. Proc. Natl. Acad. Sci. U. S. A. 110,
628 7506–11. doi:10.1073/pnas.1301251110

629 Boucher, M.J., Ghosh, S., Zhang, L., Lal, A., Jang, S.W., Ju, A., Zhang, S., Wang, X.,
630 Ralph, S.A., Zou, J., Elias, J.E., Yeh, E., 2018. Integrative proteomics and
631 bioinformatic prediction enable a high-confidence apicoplast proteome in malaria
632 parasites. PLoS Biol. 16, e2005895. doi:10.1371/journal.pbio.2005895

633 Bozdech, Z., Llinás, M., Pulliam, B.L., Wong, E.D., Zhu, J., DeRisi, J.L., 2003. The
634 transcriptome of the intraerythrocytic developmental cycle of *Plasmodium*
635 *falciparum*. PLoS Biol. 1, E5. doi:10.1371/journal.pbio.0000005

636 Bryk, R., Lima, C.D., Erdjument-Bromage, H., Tempst, P., Nathan, C., 2002. Metabolic
637 enzymes of mycobacteria linked to antioxidant defense by a thioredoxin-like
638 protein. Science 295, 1073–7. doi:10.1126/science.1067798

639 Bunik, V., Follmann, H., 1993. Thioredoxin reduction dependent on alpha-ketoacid
640 oxidation by alpha-ketoacid dehydrogenase complexes. FEBS Lett. 336, 197–
641 200. doi:10.1016/0014-5793(93)80801-Z

642 Bushell, E., Gomes, A.R., Sanderson, T., Anar, B., Girling, G., Herd, C., Metcalf, T.,
643 Modrzynska, K., Schwach, F., Martin, R.E., Mather, M.W., McFadden, G.I., Parts,
644 L., Rutledge, G.G., Vaidya, A.B., Wengelnik, K., Rayner, J.C., Billker, O., 2017.
645 Functional Profiling of a *Plasmodium* Genome Reveals an Abundance of
646 Essential Genes. Cell 170, 260-272.e8. doi:10.1016/j.cell.2017.06.030

647 Chan, M., Sim, T.-S., 2005. Functional analysis, overexpression, and kinetic

characterization of pyruvate kinase from *Plasmodium falciparum*. Biochem. Biophys. Res. Commun. 326, 188–96. doi:10.1016/j.bbrc.2004.11.018

Chokkathukalam, A., Jankevics, A., Creek, D.J., Achcar, F., Barrett, M.P., Breitling, R., 2013. mzMatch-ISO: an R tool for the annotation and relative quantification of isotope-labelled mass spectrometry data. Bioinformatics 29, 281–3. doi:10.1093/bioinformatics/bts674

Cobbold, S.A., Santos, J.M., Ochoa, A., Perlman, D.H., Llinás, M., 2016. Proteome-wide analysis reveals widespread lysine acetylation of major protein complexes in the malaria parasite. Sci. Rep. 6, 19722. doi:10.1038/srep19722

Cobbold, S.A., Vaughan, A.M., Lewis, I.A., Painter, H.J., Camargo, N., Perlman, D.H., Fishbaugher, M., Healer, J., Cowman, A.F., Kappe, S.H.I., Llinás, M., 2013. Kinetic flux profiling elucidates two independent acetyl-CoA biosynthetic pathways in *Plasmodium falciparum*. J. Biol. Chem. 288, 36338–50. doi:10.1074/jbc.M113.503557

Crawford, M.J., Thomsen-Zieger, N., Ray, M., Schachtner, J., Roos, D.S., Seeber, F., 2006. *Toxoplasma gondii* scavenges host-derived lipoic acid despite its de novo synthesis in the apicoplast. EMBO J. doi:10.1038/sj.emboj.7601189

Deponte, M., Becker, K., 2005. Glutathione S-transferase from malarial parasites: structural and functional aspects. Methods Enzymol. 401, 241–53. doi:10.1016/S0076-6879(05)01015-3

Dietz, K.-J., Turkan, I., Krieger-Liszkay, A., 2016. Redox- and Reactive Oxygen Species-Dependent Signaling into and out of the Photosynthesizing Chloroplast. Plant Physiol. 171, 1541–50. doi:10.1104/pp.16.00375

671 Dockrell, H.M., Playfair, J.H., 1984. Killing of *Plasmodium yoelii* by enzyme-induced
672 products of the oxidative burst. Infect. Immun. 43, 451–6.

673 Falkard, B., Kumar, T.R.S., Hecht, L.-S., Matthews, K.A., Henrich, P.P., Gulati, S.,
674 Lewis, R.E., Manary, M.J., Winzeler, E.A., Sinnis, P., Prigge, S.T., Heussler, V.,
675 Deschermeier, C., Fidock, D.A., 2013. A key role for lipoic acid synthesis during
676 *Plasmodium* liver stage development. Cell. Microbiol. 15, 1585–604.
677 doi:10.1111/cmi.12137

678 Feeney, M.A., Veeravalli, K., Boyd, D., Gon, S., Faulkner, M.J., Georgiou, G.,
679 Beckwith, J., 2011. Repurposing lipoic acid changes electron flow in two important
680 metabolic pathways of *Escherichia coli*. Proc. Natl. Acad. Sci. U. S. A. 108, 7991–
681 6. doi:10.1073/pnas.1105429108

682 Foth, B.J., Stimmler, L.M., Handman, E., Crabb, B.S., Hodder, A.N., McFadden, G.I.,
683 2005. The malaria parasite Plasmodium falciparum has only one pyruvate
684 dehydrogenase complex, which is located in the apicoplast. Mol. Microbiol. 55,
685 39–53. doi:10.1111/j.1365-2958.2004.04407.x

686 Frohnecke, N., Klein, S., Seeber, F., 2015. Protein-protein interaction studies provide
687 evidence for electron transfer from ferredoxin to lipoic acid synthase in
688 *Toxoplasma gondii*. FEBS Lett. 589, 31–6. doi:10.1016/j.febslet.2014.11.020

689 Gamo, F.-J., Sanz, L.M., Vidal, J., de Cozar, C., Alvarez, E., Lavandera, J.-L.,
690 Vanderwall, D.E., Green, D.V.S., Kumar, V., Hasan, S., Brown, J.R., Peishoff,
691 C.E., Cardon, L.R., Garcia-Bustos, J.F., 2010. Thousands of chemical starting
692 points for antimalarial lead identification. Nature 465, 305–10.
693 doi:10.1038/nature09107

694 Goodyer, I.D., Taraschi, T.F., 1997. *Plasmodium falciparum*: A Simple, Rapid Method
695 for Detecting Parasite Clones in Microtiter Plates. Exp. Parasitol. 86, 158–160.
696 doi:10.1006/EXPR.1997.4156

697 Gorąca, A., Huk-Kolega, H., Piechota, A., Kleniewska, P., Ciejka, E., Skibska, B.,
698 2011. Lipoic acid - biological activity and therapeutic potential. Pharmacol. Rep.
699 63, 849–58. doi:10.1016/S1734-1140(11)70600-4

700 Graves, P.M., Carter, R., McNeill, K.M., 1984. Gametocyte production in cloned lines
701 of *Plasmodium falciparum*. Am. J. Trop. Med. Hyg. 33, 1045–50.
702 doi:10.4269/ajtmh.1984.33.1045

703 Guggisberg, A.M., Frasse, P.M., Jezewski, A.J., Kafai, N.M., Gandhi, A.Y., Erlinger,
704 S.J., Odom John, A.R., 2018. Suppression of Drug Resistance Reveals a Genetic
705 Mechanism of Metabolic Plasticity in Malaria Parasites. MBio 9, 1–16.
706 doi:10.1128/mBio.01193-18

707 Günther, S., Storm, J., Müller, S., 2009. *Plasmodium falciparum*: organelle-specific
708 acquisition of lipoic acid. Int. J. Biochem. Cell Biol. 41, 748–52.
709 doi:10.1016/j.biocel.2008.10.028

710 Günther, S., Wallace, L., Patzewitz, E.-M., McMillan, P.J., Storm, J., Wrenger, C.,
711 Bissett, R., Smith, T.K., Müller, S., 2007. Apicoplast lipoic acid protein ligase B is
712 not essential for *Plasmodium falciparum*. PLoS Pathog. 3, e189.
713 doi:10.1371/journal.ppat.0030189

714 Haramaki, N., Han, D., Handelman, G.J., Tritschler, H.J., Packer, L., 1997. Cytosolic
715 and mitochondrial systems for NADH- and NADPH-dependent reduction of alpha-
716 lipoic acid. Free Radic. Biol. Med. 22, 535–42. doi:10.1016/S0891-

5849(96)00400-5

Harris, M.T., Walker, D.M., Drew, M.E., Mitchell, W.G., Dao, K., Schroeder, C.E., Flaherty, D.P., Weiner, W.S., Golden, J.E., Morris, J.C., 2013. Interrogating a hexokinase-selected small-molecule library for inhibitors of *Plasmodium falciparum* hexokinase. Antimicrob. Agents Chemother. 57, 3731–7. doi:10.1128/AAC.00662-13

Harwaldt, P., Rahlfs, S., Becker, K., 2002. Glutathione S-transferase of the malarial parasite *Plasmodium falciparum*: characterization of a potential drug target. Biol. Chem. 383, 821–30. doi:10.1515/BC.2002.086

Heneberg, P., 2018. Redox Regulation of Hexokinases, Antioxidants & Redox Signaling. Mary Ann Liebert, Inc., New York . doi:10.1089/ars.2017.7255

Jankevics, A., Merlo, M.E., de Vries, M., Vonk, R.J., Takano, E., Breitling, R., 2012. Separating the wheat from the chaff: a prioritisation pipeline for the analysis of metabolomics datasets. Metabolomics 8, 29–36. doi:10.1007/s11306-011-0341-0

Kagan, V.E., Shvedova, A., Serbinova, E., Khan, S., Swanson, C., Powell, R., Packer, L., 1992. Dihydrolipoic acid-a universal antioxidant both in the membrane and in the aqueous phase. Reduction of peroxyl, ascorbyl and chromanoxyl radicals. Biochem. Pharmacol. doi:10.1016/0006-2952(92)90482-X

Ke, H., Lewis, I.A., Morrisey, J.M., McLean, K.J., Ganesan, S.M., Painter, H.J., Mather, M.W., Jacobs-Lorena, M., Llinás, M., Vaidya, A.B., 2015. Genetic investigation of tricarboxylic acid metabolism during the *Plasmodium falciparum* life cycle. Cell Rep. 11, 164–74. doi:10.1016/j.celrep.2015.03.011

740 Kehr, S., Sturm, N., Rahlfs, S., Przyborski, J.M., Becker, K., 2010. Compartmentation
741 of redox metabolism in malaria parasites. PLoS Pathog. 6, e1001242.
742 doi:10.1371/journal.ppat.1001242

743 Kimata-Ariga, Y., Yuasa, S., Saitoh, T., Fukuyama, H., Hase, T., 2018. *Plasmodium*-
744 specific basic amino acid residues important for the interaction with ferredoxin on
745 the surface of ferredoxin-NADP+ reductase. J. Biochem. 164, 231–237.
746 doi:10.1093/jb/mvy045

747 Krnajski, Z., Walter, R.D., Müller, S., 2001. Isolation and functional analysis of two
748 thioredoxin peroxidases (peroxiredoxins) from *Plasmodium falciparum*. Mol.
749 Biochem. Parasitol. 113, 303–308. doi:10.1016/S0166-6851(01)00219-5

750 Laine, L.M., Biddau, M., Byron, O., Müller, S., 2015. Biochemical and structural
751 characterization of the apicoplast dihydrolipoamide dehydrogenase of
752 *Plasmodium falciparum*. Biosci. Rep. 35, 1–15. doi:10.1042/BSR20140150

753 Lambros, C., Vanderberg, J.P., 1979. Synchronization of *Plasmodium falciparum*
754 erythrocytic stages in culture. J. Parasitol. 65, 418–20.

755 Liebau, E., Bergmann, B., Campbell, A.M., Teesdale-Spittle, P., Brophy, P.M.,
756 Lüersen, K., Walter, R.D., 2002. The glutathione S-transferase from *Plasmodium*
757 *falciparum*. Mol. Biochem. Parasitol. 124, 85–90. doi:10.1016/S0166-
758 6851(02)00160-3

759 Lim, L., McFadden, G.I., 2010. The evolution, metabolism and functions of the
760 apicoplast. Philos. Trans. R. Soc. Lond. B. Biol. Sci. 365, 749–63.
761 doi:10.1098/rstb.2009.0273

762 Lindner, S.E., Mikolajczak, S.A., Vaughan, A.M., Moon, W., Joyce, B.R., Sullivan,

763 W.J., Kappe, S.H.I., 2013. Perturbations of *Plasmodium* Puf2 expression and
764 RNA-seq of Puf2-deficient sporozoites reveal a critical role in maintaining RNA
765 homeostasis and parasite transmissibility. Cell. Microbiol. 15, 1266–83.
766 doi:10.1111/cmi.12116

767 Livak, K.J., Schmittgen, T.D., 2001. Analysis of relative gene expression data using
768 real-time quantitative PCR and the 2(-Delta Delta C(T)) Method. Methods 25,
769 402–8. doi:10.1006/meth.2001.1262

770 MacRae, J.I., Dixon, M.W., Dearnley, M.K., Chua, H.H., Chambers, J.M., Kenny, S.,
771 Bottova, I., Tilley, L., McConville, M.J., 2013. Mitochondrial metabolism of sexual
772 and asexual blood stages of the malaria parasite *Plasmodium falciparum*. BMC
773 Biol. 11, 67. doi:10.1186/1741-7007-11-67

774 Maier, A.G., Braks, J.A.M., Waters, A.P., Cowman, A.F., 2006. Negative selection
775 using yeast cytosine deaminase/uracil phosphoribosyl transferase in *Plasmodium*
776 *falciparum* for targeted gene deletion by double crossover recombination. Mol.
777 Biochem. Parasitol. 150, 118–21. doi:10.1016/j.molbiopara.2006.06.014

778 McMillan, P.J., Stimmler, L.M., Foth, B.J., McFadden, G.I., Müller, S., 2005. The
779 human malaria parasite *Plasmodium falciparum* possesses two distinct
780 dihydrolipoamide dehydrogenases. Mol. Microbiol. 55, 27–38.
781 doi:10.1111/j.1365-2958.2004.04398.x

782 Millard, P., Delépine, B., Guionnet, M., Heuillet, M., Bellvert, F., Létisse, F., Wren, J.,
783 2019. IsoCor: Isotope correction for high-resolution MS labeling experiments.
784 Bioinformatics 35, 4484–4487. doi:10.1093/bioinformatics/btz209

785 Mohring, F., Pretzel, J., Jortzik, E., Becker, K., 2014. The redox systems of

Plasmodium falciparum and *Plasmodium vivax*: comparison, in silico analyses and inhibitor studies. Curr. Med. Chem. 21, 1728–56.

Mohring, F., Rahbari, M., Zechmann, B., Rahlfs, S., Przyborski, J.M., Meyer, A.J., Becker, K., 2017. Determination of glutathione redox potential and pH value in subcellular compartments of malaria parasites. Free Radic. Biol. Med. 104, 104–117. doi:10.1016/j.freeradbiomed.2017.01.001

Mony, B.M., Mehta, M., Jarori, G.K., Sharma, S., 2009. Plant-like phosphofructokinase from *Plasmodium falciparum* belongs to a novel class of ATP-dependent enzymes. Int. J. Parasitol. 39, 1441–53. doi:10.1016/j.ijpara.2009.05.011

Mooney, B.P., Miernyk, J.A., Randall, D.D., 2002. The complex fate of alpha-ketoacids. Annu. Rev. Plant Biol. 53, 357–75. doi:10.1146/annurev.arplant.53.100301.135251

Moura, F.A., de Andrade, K.Q., dos Santos, J.C.F., Goulart, M.O.F., 2015. Lipoic Acid: its antioxidant and anti-inflammatory role and clinical applications. Curr. Top. Med. Chem. 15, 458–83. doi:10.2174/1568026615666150114161358

Müller, S., 2015. Role and Regulation of Glutathione Metabolism in *Plasmodium falciparum*. Molecules 20, 10511–34. doi:10.3390/molecules200610511

Nepveu, F., Turrini, F., 2013. Targeting the redox metabolism of *Plasmodium falciparum*. Future Med. Chem. doi:10.4155/fmc.13.159

Nietzel, T., Mostertz, J., Hochgräfe, F., Schwarzländer, M., 2017. Redox regulation of mitochondrial proteins and proteomes by cysteine thiol switches. Mitochondrion 33, 72–83. doi:10.1016/j.mito.2016.07.010

O'Neill, M.T., Phuong, T., Healer, J., Richard, D., Cowman, A.F., O'Neill, M.T., Phuong, T., Healer, J., Richard, D., Cowman, A.F., 2011. Gene deletion from *Plasmodium falciparum* using FLP and Cre recombinases: Implications for applied site-specific recombination. Int. J. Parasitol. 41, 117–123.

Oppenheim, R.D., Creek, D.J., Macrae, J.I., Modrzynska, K.K., Pino, P., Limenitakis, J., Polonais, V., Seeber, F., Barrett, M.P., Billker, O., McConville, M.J., Soldati-Favre, D., 2014. BCKDH: The Missing Link in Apicomplexan Mitochondrial Metabolism Is Required for Full Virulence of *Toxoplasma gondii* and *Plasmodium berghei*. PLoS Pathog. doi:10.1371/journal.ppat.1004263

Packer, L., Witt, E.H., Tritschler, H.J., 1995. alpha-Lipoic acid as a biological antioxidant. Free Radic. Biol. Med. 19, 227–50. doi:10.1016/0891-5849(95)00017-R

Pastrana-Mena, R., Dinglasan, R.R., Franke-Fayard, B., Vega-Rodríguez, J., Fuentes-Caraballo, M., Baerga-Ortiz, A., Coppens, I., Jacobs-Lorena, M., Janse, C.J., Serrano, A.E., 2010. Glutathione reductase-null malaria parasites have normal blood stage growth but arrest during development in the mosquito. J. Biol. Chem. 285, 27045–27056. doi:10.1074/jbc.M110.122275

Patzewitz, E.-M., Salcedo-Sora, J.E., Wong, E.H., Sethia, S., Stocks, P.A., Maughan, S.C., Murray, J.A.H., Krishna, S., Bray, P.G., Ward, S.A., Müller, S., 2013. Glutathione Transport: A New Role for PfCRT in Chloroquine Resistance. Antioxid. Redox Signal. doi:10.1089/ars.2012.4625

Perham, R.N., 2000. Swinging arms and swinging domains in multifunctional enzymes: catalytic machines for multistep reactions. Annu. Rev. Biochem. 69,

961–1004. doi:10.1146/annurev.biochem.69.1.961

Pick, U., Haramaki, N., Constantinescu, A., Handelman, G.J., Tritschler, H.J., Packer, L., 1995. Glutathione reductase and lipoamide dehydrogenase have opposite stereospecificities for alpha-lipoic acid enantiomers. Biochem. Biophys. Res. Commun. 206, 724–30. doi:10.1006/bbrc.1995.1102

Ponnudurai, T., Lensen, A.H.W., Meis, J.F.G.M., Meuwissen, J.H.E., 1986. Synchronization of *Plasmodium falciparum* gametocytes using an automated suspension culture system. Parasitology 93 (Pt 2), 263–74. doi:10.1017/S003118200005143X

Rahbari, M., Rahlfs, S., Przyborski, J.M., Schuh, A.K., Hunt, N.H., Fidock, D.A., Grau, G.E., Becker, K., 2017. Hydrogen peroxide dynamics in subcellular compartments of malaria parasites using genetically encoded redox probes. Sci. Rep. doi:10.1038/s41598-017-10093-8

Rungsiwongse, J., Rosenberg, R., 1991. The Number of Sporozoites Produced by Individual Malaria Oocysts. Am. J. Trop. Med. Hyg. 45, 574–577. doi:10.4269/ajtmh.1991.45.574

Salcedo-Sora, J.E., Caamano-Gutierrez, E., Ward, S.A., Biagini, G.A., 2014. The proliferating cell hypothesis: A metabolic framework for *Plasmodium* growth and development. Trends Parasitol. doi:10.1016/j.pt.2014.02.001

Scheltema, R.A., Jankevics, A., Jansen, R.C., Swertz, M.A., Breitling, R., 2011. PeakML/mzMatch: a file format, Java library, R library, and tool-chain for mass spectrometry data analysis. Anal. Chem. 83, 2786–93. doi:10.1021/ac2000994

Schmidtmann, E., König, A.-C., Orwat, A., Leister, D., Hartl, M., Finkemeier, I., 2014.

Redox regulation of *Arabidopsis* mitochondrial citrate synthase. Mol. Plant 7, 156–69. doi:10.1093/mp/sst144

Seeber, F., Aliverti, A., Zanetti, G., 2005. The Plant-Type Ferredoxin-NADP+ Reductase/Ferredoxin Redox System as a Possible Drug Target Against Apicomplexan Human Parasites. Curr. Pharm. Des. 11, 3159–3172. doi:10.2174/1381612054864957

Seeber, F., Soldati-Favre, D., 2010. Metabolic pathways in the apicoplast of apicomplexa. Int. Rev. Cell Mol. Biol. 281, 161–228. doi:10.1016/S1937-6448(10)81005-6

Sewelam, N., Jaspert, N., Van Der Kelen, K., Tognetti, V.B., Schmitz, J., Frerigmann, H., Stahl, E., Zeier, J., Van Breusegem, F., Maurino, V.G., 2014. Spatial H2O2 signaling specificity: H2O2 from chloroplasts and peroxisomes modulates the plant transcriptome differentially. Mol. Plant 7, 1191–210. doi:10.1093/mp/ssu070

Sheiner, L., Demerly, J.L., Poulsen, N., Beatty, W.L., Lucas, O., Behnke, M.S., White, M.W., Striepen, B., 2011. A systematic screen to discover and analyze apicoplast proteins identifies a conserved and essential protein import factor. PLoS Pathog. 7, e1002392. doi:10.1371/journal.ppat.1002392

Sheiner, L., Vaidya, A.B., McFadden, G.I., 2013. The metabolic roles of the endosymbiotic organelles of *Toxoplasma* and *Plasmodium* spp. Curr. Opin. Microbiol. 16, 452–8. doi:10.1016/j.mib.2013.07.003

Shimizu, S., Osada, Y., Kanazawa, T., Tanaka, Y., Arai, M., 2010. Suppressive effect of azithromycin on *Plasmodium berghei* mosquito stage development and apicoplast replication. doi:10.1186/1475-2875-9-73

877 Shivapurkar, R., Hingamire, T., Kulkarni, A.S., Rajamohanan, P.R., Reddy, D.S.,
878 Shanmugam, D., 2018. Evaluating antimalarial efficacy by tracking glycolysis in
879 *Plasmodium falciparum* using NMR spectroscopy. Sci. Rep. 8, 1–10.
880 doi:10.1038/s41598-018-36197-3

881 Siciliano, G., Santha Kumar, T.R., Bona, R., Camarda, G., Calabretta, M.M., Cevenini,
882 L., Davioud-Charvet, E., Becker, K., Cara, A., Fidock, D.A., Alano, P., 2017. A
883 high susceptibility to redox imbalance of the transmissible stages of *Plasmodium*
884 *falciparum* revealed with a luciferase-based mature gametocyte assay. Mol.
885 Microbiol. 104, 306–318. doi:10.1111/mmi.13626

886 Storm, J., Sethia, S., Blackburn, G.J., Chokkathukalam, A., Watson, D.G., Breitling,
887 R., Coombs, G.H., Müller, S., 2014. Phosphoenolpyruvate carboxylase identified
888 as a key enzyme in erythrocytic *Plasmodium falciparum* carbon metabolism.
889 PLoS Pathog. 10, e1003876. doi:10.1371/journal.ppat.1003876

890 Sumner, L.W., Amberg, A., Barrett, D., Beale, M.H., Beger, R., Daykin, C.A., Fan,
891 T.W.M., Fiehn, O., Goodacre, R., Griffin, J.L., Hankemeier, T., Hardy, N., Harnly,
892 J., Higashi, R., Kopka, J., Lane, A.N., Lindon, J.C., Marriott, P., Nicholls, A.W.,
893 Reily, M.D., Thaden, J.J., Viant, M.R., 2007. Proposed minimum reporting
894 standards for chemical analysis: Chemical Analysis Working Group (CAWG)
895 Metabolomics Standards Initiative (MSI). Metabolomics. doi:10.1007/s11306-
896 007-0082-2

897 Tautenhahn, R., Bottcher, C., Neumann, S., 2008. Highly sensitive feature detection
898 for high resolution LC/MS. BMC Bioinformatics. doi:10.1186/1471-2105-9-504

899 Tibullo, D., Li Volti, G., Giallongo, C., Grasso, S., Tomassoni, D., Anfuso, C.D., Lupo,

900 G., Amenta, F., Avola, R., Bramanti, V., 2017. Biochemical and clinical relevance
901 of alpha lipoic acid: antioxidant and anti-inflammatory activity, molecular
902 pathways and therapeutic potential. Inflamm. Res. 66, 947–959.
903 doi:10.1007/s00011-017-1079-6

904 Trager, W., Jensen, J.B., 1976. Human malaria parasites in continuous culture.
905 Science 193, 673–5. doi:10.1038/098448b0

906 Urscher, M., Przyborski, J.M., Imoto, M., Deponte, M., 2010. Distinct subcellular
907 localization in the cytosol and apicoplast, unexpected dimerization and inhibition
908 of *Plasmodium falciparum* glyoxalases. Mol. Microbiol. 76, 92–103.
909 doi:10.1111/j.1365-2958.2010.07082.x

910 van Schaijk, B.C.L., Kumar, T.R.S., Vos, M.W., Richman, A., van Gemert, G.-J., Li, T.,
911 Eappen, A.G., Williamson, K.C., Morahan, B.J., Fishbaugher, M., Kennedy, M.,
912 Camargo, N., Khan, S.M., Janse, C.J., Sim, K.L., Hoffman, S.L., Kappe, S.H.I.,
913 Sauerwein, R.W., Fidock, D.A., Vaughan, A.M., 2014. Type II fatty acid
914 biosynthesis is essential for *Plasmodium falciparum* sporozoite development in
915 the midgut of *Anopheles* mosquitoes. Eukaryot. Cell 13, 550–9.
916 doi:10.1128/EC.00264-13

917 Vaughan, A.M., O'Neill, M.T., Tarun, A.S., Camargo, N., Phuong, T.M., Aly, A.S.I.,
918 Cowman, A.F., Kappe, S.H.I., 2009. Type II fatty acid synthesis is essential only
919 for malaria parasite late liver stage development. Cell. Microbiol. 11, 506–20.
920 doi:10.1111/j.1462-5822.2008.01270.x

921 Vincent, I.M., Barrett, M.P., 2015. Metabolomic-based strategies for anti-parasite drug
922 discovery. J. Biomol. Screen. doi:10.1177/1087057114551519

923 Wezena, C.A., Alisch, R., Golzmann, A., Liedgens, L., Staudacher, V., Pradel, G.,
924 Deponte, M., 2017. The cytosolic glyoxalases of *Plasmodium falciparum* are
925 dispensable during asexual blood-stage development. Microb. cell (Graz, Austria)
926 5, 32–41. doi:10.15698/mic2018.01.608

927 World Health Organization, 2019. World Malaria Report 2019. Geneva.

928 Wrenger, C., Müller, S., 2003. Isocitrate dehydrogenase of *Plasmodium falciparum*:
929 Energy metabolism or redox control? Eur. J. Biochem. doi:10.1046/j.1432-
930 1033.2003.03536.x

931 Yhe, E., and DeRisi, JL., Chemical Rescue of Malaria Parasites Lacking an Apicoplast
932 Defines Organelle Function in Blood-Stage *Plasmodium Falciparum.* PLoS Biol .
933 2011 Aug;9(8):e1001138. doi: 10.1371/journal.pbio.1001138.

934 Yoshida, K., Hisabori, T., 2014. Mitochondrial isocitrate dehydrogenase is inactivated
935 upon oxidation and reactivated by thioredoxin-dependent reduction in
936 *Arabidopsis*. Front. Environ. Sci. 2, 1–7. doi:10.3389/fenvs.2014.00038

937 Yoshida, K., Noguchi, K., Motohashi, K., Hisabori, T., 2013. Systematic exploration of
938 thioredoxin target proteins in plant mitochondria. Plant Cell Physiol.
939 doi:10.1093/pcp/pct037

940 Zhang, M., Wang, C., Otto, T.D., Oberstaller, J., Liao, X., Adapa, S.R., Udenze, K.,
941 Bronner, I.F., Casandra, D., Mayho, M., Brown, J., Li, S., Swanson, J., Rayner,
942 J.C., Jiang, R.H.Y., Adams, J.H., 2018. Uncovering the essential genes of the
943 human malaria parasite *Plasmodium falciparum* by saturation mutagenesis.
944 Science 360, eaap7847. doi:10.1126/science.aap7847

945 Zocher, K., Fritz-Wolf, K., Kehr, S., Fischer, M., Rahlfs, S., Becker, K., 2012.

946 Biochemical and structural characterization of *Plasmodium falciparum* glutamate
947 dehydrogenase 2. Mol. Biochem. Parasitol. 183, 52–62.
948 doi:10.1016/j.molbiopara.2012.01.007

949 Zuzarte-Luís, V., Mello-Vieira, J., Marreiros, I.M., Liehl, P., Chora, Â.F., Carret, C.K.,
950 Carvalho, T., Mota, M.M., 2017. Dietary alterations modulate susceptibility to
951 *Plasmodium* infection. Nat. Microbiol. 2, 1600–1607. doi:10.1038/s41564-017-
952 0025-2

953

954

955 **Figure legends**

956 **Fig. 1**. Schematic representation of Pyruvate Dehydrogenase Complex (PDC) and Lipoic Acid
957 (LA) biosynthesis components and function in the *Plasmodium falciparum* apicoplast. Each of
958 the PDC enzyme reactions is shown in a different colour (E1, red; E2, green; E3, blue). The
959 three states of E2-conjugated LA are depicted onto the schematic E2. ACCase, acetyl-CoA
960 carboxylase; CoA, coenzyme A; FAD, flavin adenine dinucleotide; FAS II, fatty acid
961 biosynthesis type II; LipA, lipoyl synthase; LipB, Octanoyl-ACP:protein *N*-octanoyltransferase;
962 NAD, nicotinamide adenine dinucleotide; PK, pyruvate kinase; TPP, thiamine pyrophosphate.

963

964 **Fig. 2.** Analysis of *Plasmodium falciparum* apicoplast antioxidant relative expression levels
965 and cytosolic antioxidant relative protein levels. (A) Relative transcript levels for apicoplast
966 antioxidant protein (AOP), glutathione peroxidase-like thioredoxin peroxidase (TPx_{Gl}), and
967 apicoplast thioredoxin-like protein 2 (ATrx2), in the lipoic acid protein ligase B (LipB) mutant
968 compared with wild type. Parasites were highly synchronised following the sorbitol and
969 magnetic activated cell sorting (MACS) protocol (see section 2) and harvested at 26, 30 and
970 34 h post-invasion (hpi). Differences are expressed as Log_2 of the $3D7^{\Delta PflipB}/3D7^{WT}$ ratio of the
971 mean signals from three experiments performed in triplicate (*n*=3). Error bars show S.D.
972 Variances were analysed using the two-way ANOVA test coupled with the Bonferroni test
973 using GraphPad Prism 8. Asterisks and graph lines are colour coded as shown in the legend.
974 **P*<0.05; ***P*<0.01; ****P*<0.001. (B) Relative protein levels for the cytosolic antioxidant proteins
975 GST, 1-Cys peroxiredoxin (1-CysPx) and 2-Cys peroxiredoxin (2-CysPx). Three independent
976 experiments were performed in technical triplicates and the means (*n*=2) of actin-normalised
977 fluorescent signals for each protein were calculated using quantitative fluorescent western
978 blotting. The bars represent the $3D7^{\Delta PflipB}/3D7^{WT}$ average ratio ± S.D. The variance was
979 analysed with the Student's *t*-test using GraphPad Prism 8. **P*<0.01. KO, knockout; WT, wild
980 type. (C) The variation for each parasite stage during asexual development was estimated by

counting 200 random infected red blood cells (RBCs) for each time point for 3D7^{WT} (a) and 3D7$^{\Delta PflipB}$ mutants (b). Fractions are presented as the mean percentage from three cultures for each condition; error bars correspond to S.D. (D) The graph represents the number of merozoites per 'segmenter' stage (*n*=100) in 3D7$^{\Delta PflipB}$ mutants and 3D7^{WT}. Bars represent mean ± S.D.

Fig. 3. Analysis of D-glucose (A) and L-lactate (B) in spent medium samples from *Plasmodium falciparum* 3D7$^{\Delta PflipB}$ mutant and 3D7^{WT} parasite cultures. Spent medium samples were collected at 30, 34, 38 and 42 h post-invasion (hpi) and analysed using a commercial enzymatic assay for D-glucose and L-lactate. Triplicate cultures at 2% parasitemia were used for each parasite line for this experiment. The mean signals from two independent experiments (*n*=2) are represented by dots in each time point. The variance between the lines at each time point was analysed with the Student's *t*-test using GraphPad Prism 8. **P*<0.05; ***P*<0.01; ****P*<0.001.

Fig. 4. Metabolomic analyses of *Plasmodium falciparum* 3D7$^{\Delta PflipB}$ mutant and 3D7^{WT} parasites using ^{13}C-U-D-glucose labelling. Results from two independent targeted metabolomics experiments in technical triplicates comparing 3D7$^{\Delta PflipB}$ mutants and 3D7^{WT} after incubation in culture medium containing 100% ^{13}C-U-D-glucose for 28 h. (A) Schematics of the *P. falciparum* central carbon metabolism pathways analysed here, highlighting the metabolic adaptations in 3D7$^{\Delta PflipB}$ mutant compared with wild-type (WT) parasites. Arrows shaded in red and blue, respectively, correspond to a decrease and increase in flux for each specific reaction. Red and black dots under metabolite names, respectively, depict the number of labelled and unlabelled carbons, based on the most abundant labelled form of the metabolite. The relative abundances of BCKDH, ICDH and PDC E2 are reported next to each reaction. Ac-CoA, acetyl-CoA; BCKDH, branched-chain ketoacid dehydrogenase; DHAP,

dihydroxyacetone phosphate; OAA, oxaloacetate; PEP, phospho*enol*pyruvate. (B,C) Relative intracellular levels for each metabolite obtained by the sum of all the peak areas for each isotopologue of a specific metabolite. The differences in abundance for each metabolite are expressed as Log_2 of the $3D7^{\Delta PflipB}/3D7^{WT}$ (B) or $Log_2(3D7^{\Delta Pfae3}/3D7^{WT})$ (C) mean ratio ± S.D. (*n*=2). (D,E) Bar graphs summarising the percentage of isotopic incorporation in each identified metabolite calculated from the chromatographic peak areas. The bars are divided to represent the mean contribution (*n*=2) of the different isotopologues to each metabolite labelled fraction and error bars are S.D. Empty bars represent metabolites identified in $3D7^{WT}$ parasites, while dashed bars correspond to metabolites from $3D7^{\Delta PflipB}$ mutants (D) or $3D7^{\Delta Pfae3}$ mutants (E). The variance in the citrate M+5 fraction between mutants and $3D7^{WT}$ is depicted by an asterisk coloured with the corresponding legend colour and was analysed with the Student's *t*-test using GraphPad Prism 8. **P*<0.05.

Fig. 5. Analysis of the expression of metabolic enzymes and the levels of cofactors involved in glycolysis and in the tricarboxylic acid (TCA) cycle of *Plasmodium falciparum*. (A) Relative protein levels for the mitochondrial enzymes branched-chain ketoacid dehydrogenase (BCKDH E2), isocitrate dehydrogenase (ICDH) and of the apicoplast enzyme dihydrolipoamide transacetylase (PDC E2). Data from three experiments performed in biological triplicates (*n*=3) are shown as the $3D7^{\Delta PflipB}$: $3D7^{WT}$ ratio of the actin-normalised mean fluorescent signals for each protein. Error bars represent S.D. The variance was analysed with the Student's *t*-test using GraphPad Prism 5. **P*<0.05. (B) Relative intracellular levels of metabolic cofactors are represented as Log_2 of the $3D7^{\Delta PflipB}$: $3D7^{WT}$ ratio of the means from two experiments in biological triplicates. The relative mean levels are the sum of all peak areas relative to each isotopologue of each metabolite (*n*=2). Error bars represent S.D. (C) (a) Bar graph summarising the percentage of isotope incorporation in the identified cofactors AMP, ADP, ATP and NAD^+. Data correspond to two experiments performed in biological triplicates (*n*=2). The bars are divided to the mean contribution of each isotopologue

to the total labelled fraction and displays error bars correspond to S.D. Empty bars correspond to metabolites identified in 3D7^{WT} parasites, while dashed bars refer to metabolites from 3D7$^{\Delta PflipB}$ mutants. The variance of each isotopologue fraction between 3D7$^{\Delta PflipB}$ and 3D7^{WT} (*n*=2) is indicated by the asterisk symbol (coloured according to legend) and was analysed with the Student's *t*-test using GraphPad Prism 8;.*P<0.05. **(**b**)** the same graph as (a) is shown with data points indicated for M+5 (orange) and M+10 (yellow).

Fig. 6. Bar graphs representing the data from Table 2. All data points are showed as dots for each bar. Error bars correspond to S.D.

Fig. 7. *Plasmodium falciparum* oocyst morphology on days 7 and 13 post-feeding of gametocytes to *Anopheles* mosquitoes shows a defect in sporozoite development for lipoic acid protein ligase B (LipB) knockout parasites. (A) Two representative light microscopy images of NF54$^{\Delta lipB}$ and of NF54^{WT} oocytes on day 7 post-feeding. Scale bars = 25 microns (B) A representative differential interference contrast (DIC) microscopy image of NF54$^{\Delta lipB}$ and of NF54^{WT} oocytes on day 13. The insets are shown in white squares. Scale bar = 25 µm. The NF54$^{\Delta PflipB}$ oocysts show malformation in both methods and time points.

Supplementary figure legends

Supplementary Fig. S1. Generation and genotypic analysis of Pf∆*lipB* in the *Plasmodium falciparum* NF54 cell line. (A) To generate parasite lines lacking a functional *pflipB* locus (PF3D7_0823600) we employed a double cross-over recombination strategy using *Cre-loxP*. Fragments (0.5 kb) on both ends of *pflipB* served as homology regions for double cross-over recombination and the LoxP site was incorporated into the genomic locus that flanks the h*dhfr* cassette. Primers used to amplify the double recombination plasmid and to test for integration are shown. (B) PCR results showing *pflipB* deletion in the knockout strain. Lane 1: marker (M) NEB 1 kb plus DNA ladder, lanes 3-4: Pf*ΔlipB*; lanes 5-6: Pf*ΔlipB*::*Cre*, lanes 7-8: wild-type NF54. Primers p5/p6 amplified a 3.6 kb fragment only from the Pf*ΔlipB* strain due to the incorporation of the h*dhfr* cassette. A much smaller 1.45 kb fragment in the Pf*ΔlipB::Cre* strain was due to the unmarking action of *Cre* recombinase. In both these strains primers p7/p8 did not give a product. Alternatively, primers p5/p6 amplified a 1.8 kb fragment in the wild-type (WT) NF54 strain. Primers p7/p8 amplified a product of 0.35 kb as the deleted fragment was retained in the non-recombinant WT NF54 strain. UTR, untranslated region.

Supplementary Fig. S2. Analysis of the *Plasmodium falciparum* apicoplast glyoxalase system enzyme relative expression levels. Relative expression levels for the enzymes glyoxalase-1-like protein (GILP) and glyoxalase 2 (tGLO) were determined in three independent experiments from highly synchronised parasites following the sorbitol and magnetic activated cell sorting (MACS) protocols (see section 2). Samples were harvested at 26, 30 and 34 h post invasion (hpi). Differences are expressed as Log_2 of the $3D7^{\Delta PflipB}$: $3D7^{WT}$ ratio of the mean signals from three experiments ± S.D. Analysis used the two-way ANOVA test coupled with the Bonferroni test using GraphPad Prism 8.

Supplementary Fig. S3. Western blot analyses of the protein levels for the cytosolic antioxidant proteins GST (A), 1-Cys peroxiredoxin (1-CysPx) (B) and 2-Cys peroxiredoxin (2-CysPx) (C) presented in Fig. 2B in the main text. Two independent experiments were performed using knockout parasites (KO1 and KO2) and each was run next to a parental control (P) in technical triplicates. Each panel includes a western blot of the gene of interest and one of the actin control.

Supplementary Fig. S4. Analysis of D-glucose (A) and L-lactate (B) in spent medium samples from 3D7$^{\Delta Pfae3}$ mutant and 3D7^{WT} parasite cultures. Spent medium samples were analysed using a commercial enzymatic assay for D-glucose and L-lactate. Three independent experiments in triplicate cultures at 4% parasitemia were used for each parasite line tested in this experiment. Results are reported as mean ± S.D. (*n*=3). The variance between the lines at each time point was analysed with the Student's *t*-test using GraphPad Prism 8. hpi, h post-invasion.

Supplementary Fig. S5. Metabolomic analyses of *Plasmodium falciparum* 3D7$^{\Delta Pfae3}$ (A,C) mutants and 3D7^{WT} (B,D) parasites using ^{13}C-U-D-glucose labelling. Results from two independent targeted metabolomics experiments in biological triplicates comparing 3D7$^{\Delta Pfae3}$ mutant and 3D7^{WT} lines after incubation in culture medium containing 100% ^{13}C-U-D-glucose for 28 h. (A-B) Heatmap representing the total labelling incorporation from ^{13}C-U-D-glucose in red blood cells (RBC), 3D7^{WT} and 3D7$^{\Delta PflipB}$ (A) or 3D7$^{\Delta Pfae3}$ (B) mutants. (C-D) Bar graphs summarising the percentage of isotopic incorporation in each identified metabolite relative to the peak area are presented including mean ± S.D. (*n*=2). Empty bars represent metabolites identified in 3D7^{WT} parasites. correspond to metabolites from 3D7$^{\Delta PflipB}$ (C) or 3D7$^{\Delta Pfae3}$ (D) mutants.

Supplementary Fig. S6. Western blots analyses of the protein levels for the *Plasmodium falciparum* mitochondrial enzymes branched-chain ketoacid dehydrogenase (PDC E2) (A), isocitrate dehydrogenase (ICDH) (B), and of the apicoplast enzyme dihydrolipoamide transacetylase (BCKDH E2) (C) presented in figure Fig. 5A in the main text. Two independent experiments were performed on knockout parasites (KO1 and KO2) and each was run next to a parental control (P) in technical triplicates. In eEach panel the includes atop western is blot of the gene of interest and the bottom one is of the actin control.

1113 **Table 1.** Percentage of solvent A and B used over time to perform LC-MS

Solvent A (%)	Solvent B (%)	Time (min)
20	80	0
80	20	30
95	5	31
95	5	35
20	80	36
20	80	46

1114

1115

1116

1117 **Table 2.** Summary of mosquito infection attempts with *Plasmodium falciparum* cell line

1118 NF54$^{\Delta PflipB}$

Stage V gametocytemia in cultures		Final concentration of stage V gametocytemia in the infectious blood meals		Wet mount exflagellation of infectious blood meal per field (x40 phase contrast)		Oocysts/mosquito		Sporozoites/ mosquito	
NF54	NF54 LipB KO	NF54	NF54 LipB KO	NF54	NF54 LipB KO	NF54	NF54 LipB KO	NF54	NF54 LipB KO*
0.40%	1.62%	0.11%	0.11%	5.2	11.7	50	32	106,543	0
1.37%	0.63%	0.12%	0.12%	8.1	6.3	36	62	150,178	0
1.45%	0.75%	0.11%	0.11%	9.3	4.9			180,991	0
0.92%	0.93%	0.10%	0.10%	1.9	2.7			109,975	0
	0.87%		0.10%		9.4		28		0
	1.10%		0.12%		5		36		0
	1.03%		0.12%		5.6		53		0
1.04% ± 0.24%	0.99% ± 0.12%	0.11% ± 0.004%	0.11% ± 0.003%	6.1 ± 1.7	6.5 ± 1.2	43.0 ± 7.0	42.2 ± 6.5	136,922 ± 17,717	0 ± 0

1119

1120 Each row represents a separate experiment, with parental NF54 included in the first four.

1121 Despite equivalent numbers of mature gametocytes and rates of exflagellation of male
1122 gametes in comparison with parental NF54 parasites, the LipB knockout (KO) parasites failed
1123 to produce any salivary gland sporozoites, as determined from dissection and counting of 20
1124 infected *Anopheles* mosquitoes per parasite line per experiment. The bottom row shows
1125 composite mean ± S.E.M. data.

Figure 1

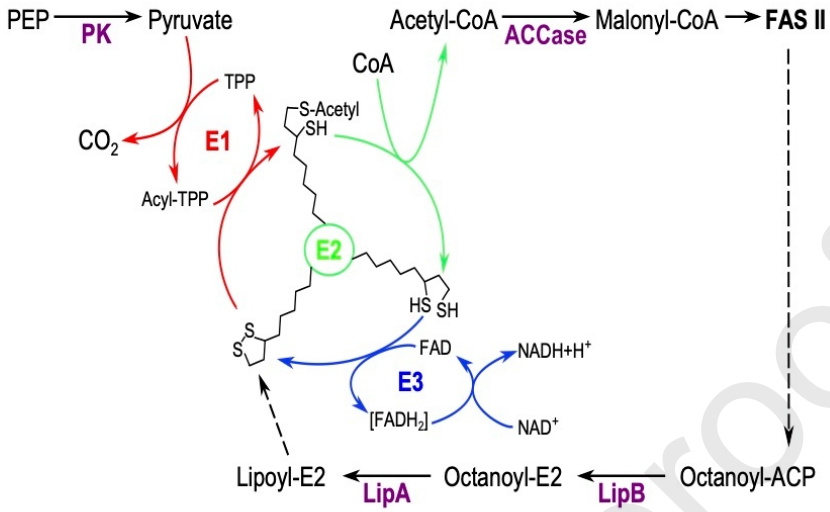

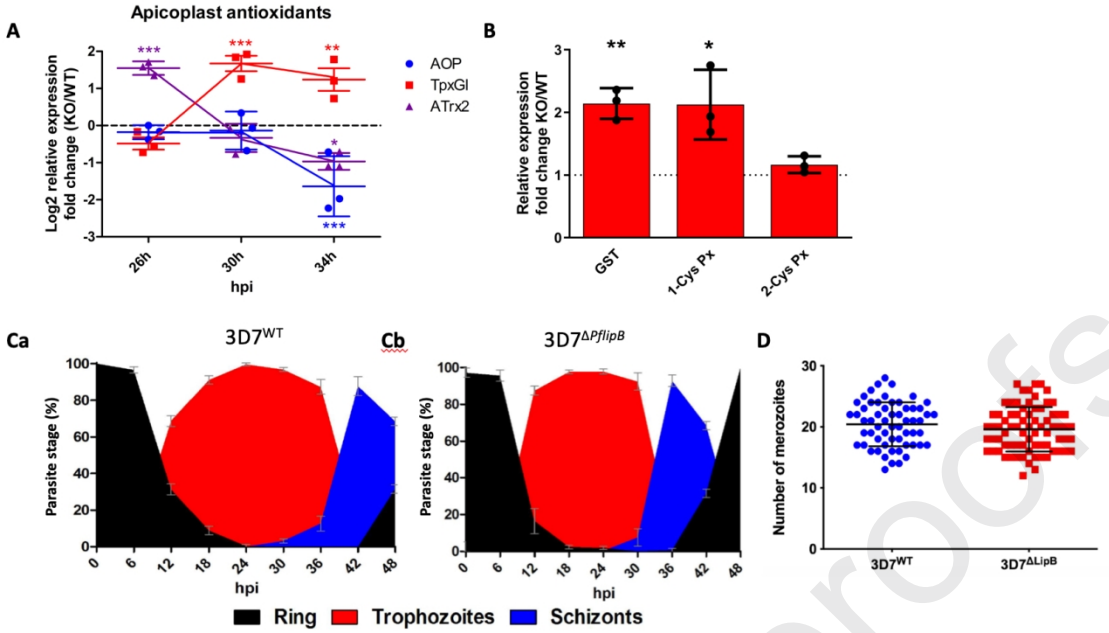

1127

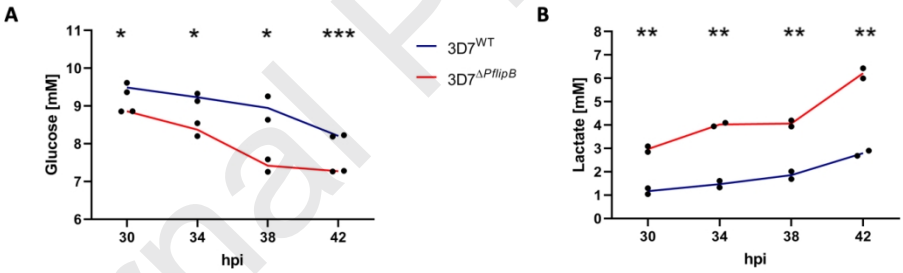

1128

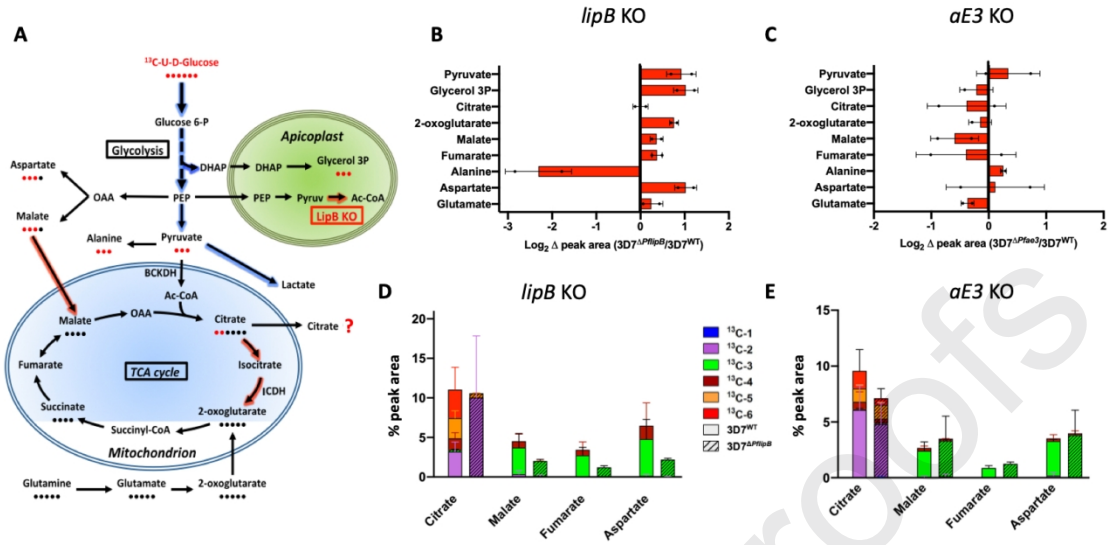

1129

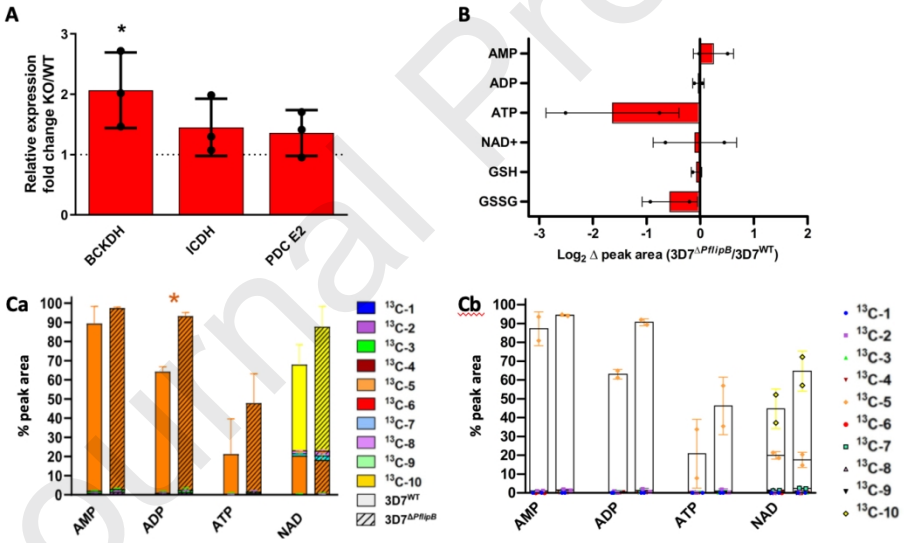

1130

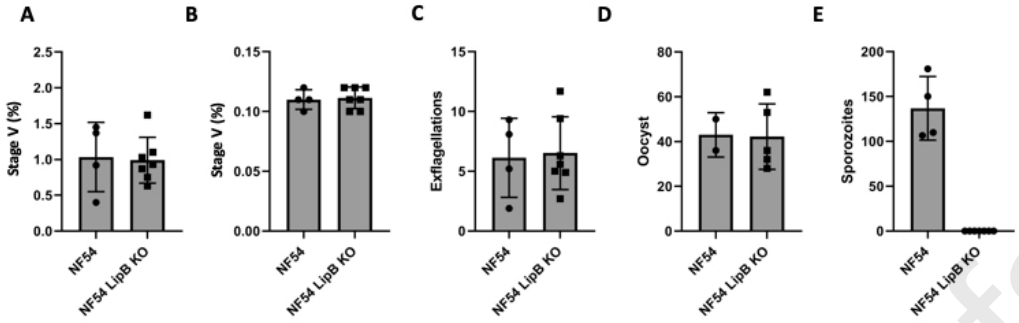

1131

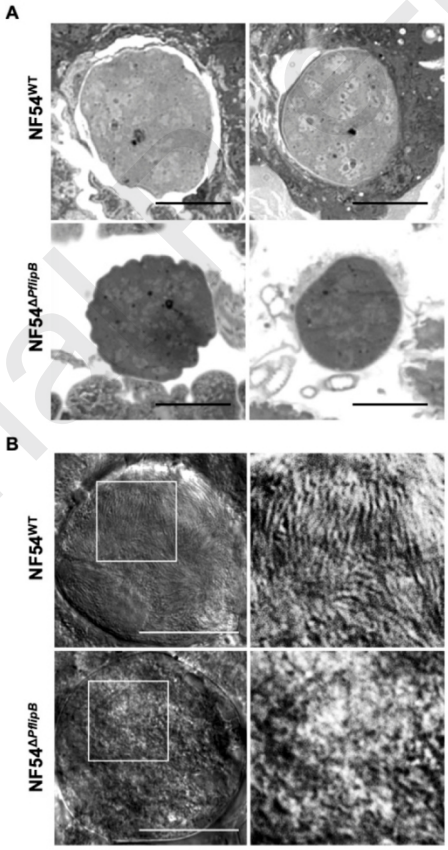

1132

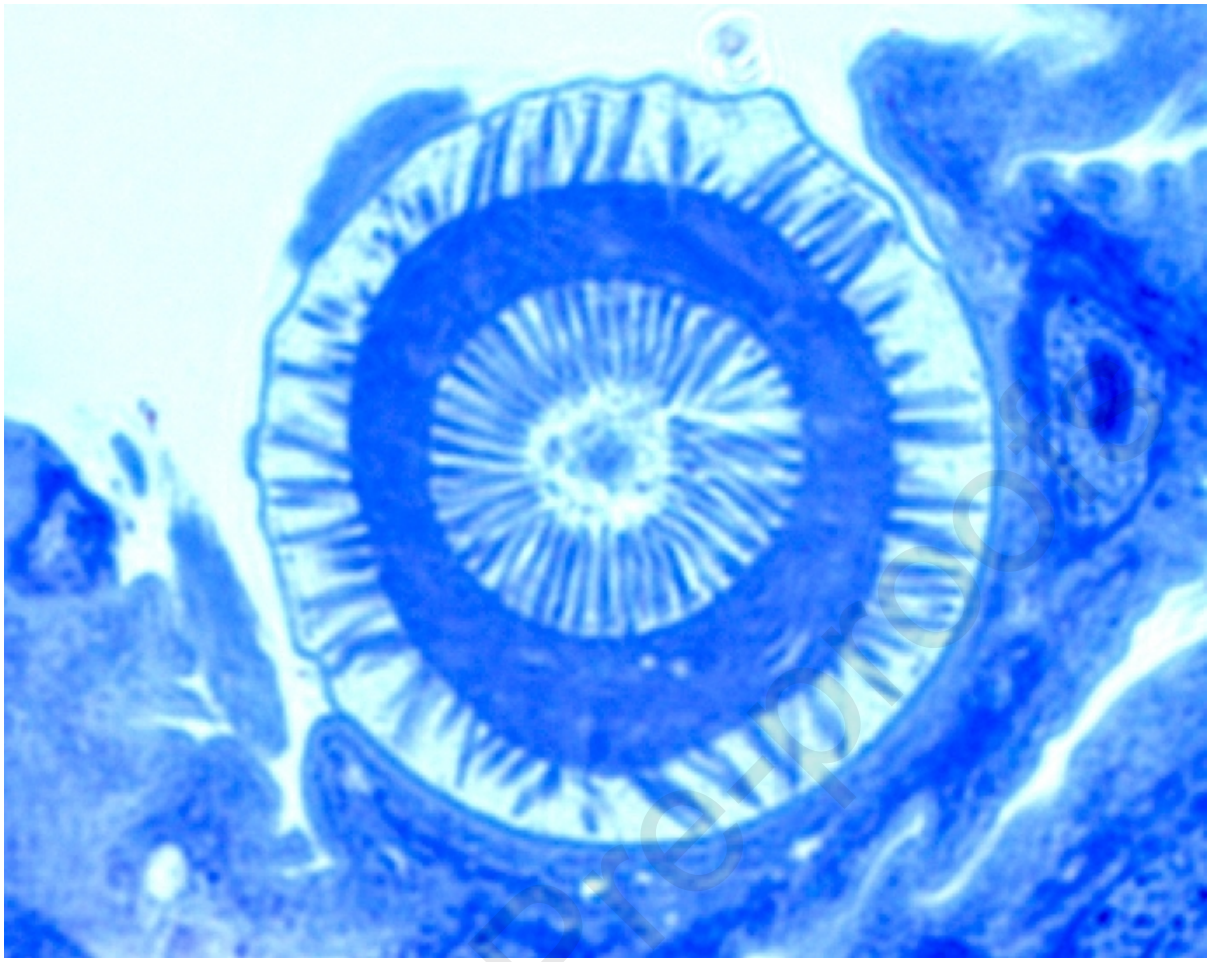

Highlights

Apicoplast LipB deletion leads to changed antioxidant expression that precedes and coincides with accelerated differentiation

3D7 *Plasmodium* exhibits changes in glycolysis and tricarboxylic acid cycle activity after deletion of apicoplast LipB

When LipB is deleted from NF54 *Plasmodium*, the resulting parasites cannot complete their development in mosquitoes

1146

1147

1148

1149

1150